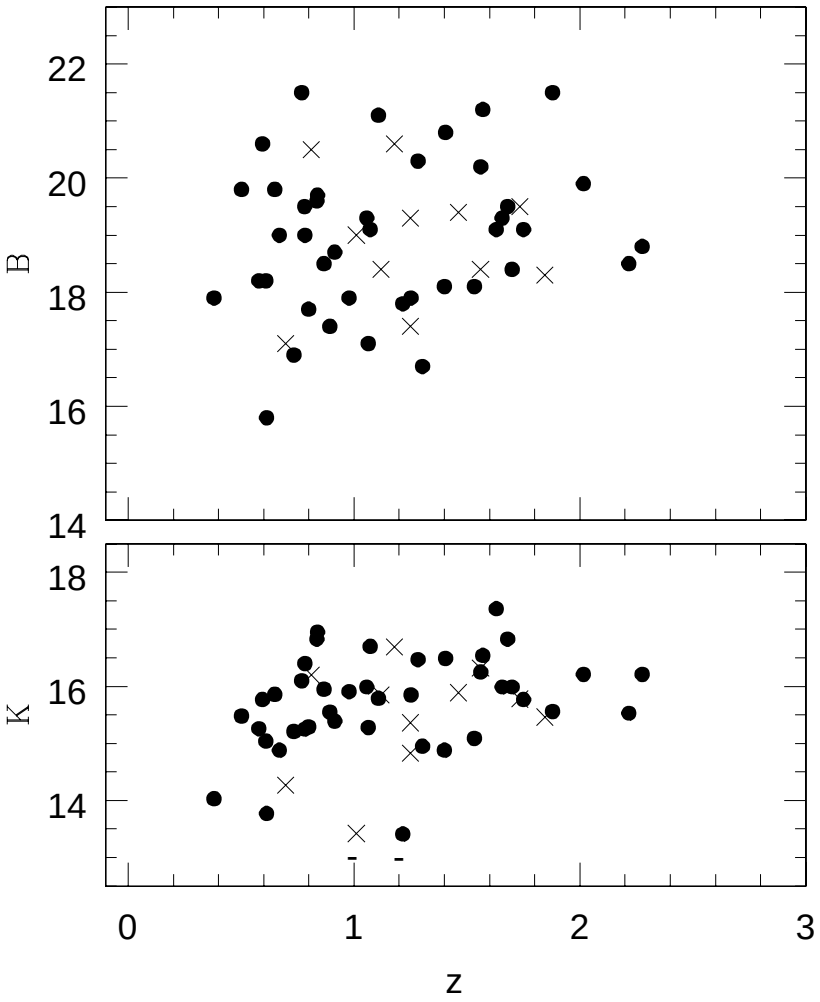
22
20
18
16
14
B
18
16
14
K
0
1
2
3
z

arXiv:astro-ph/9712220v1 17 Dec 1997

TABLE 1. The quasar sample

B3 name	z	$S_{408,\mathrm{tot}}$ Jy	$S_{1460,\mathrm{tot}}$ Jy	α_{408}^{1460}	B	R	K	$B-K$	
0701+392	1.283	1.17	0.449	-0.75	20.3	18.8	16.47	3.83	a
0704+384	0.579	2.87	0.740	-1.06	18.2	17.4	15.26	2.94	a
0726+431	1.072	1.29	0.289	-1.17	19.1	18.2	16.70	2.40	a
0739+397B	1.700	1.02	0.492	-0.57	18.4	18.0	15.99	2.41	a
0740+380C	1.063	5.55	1.067	-1.29	17.1	16.7	15.28	1.82	a
0756+406	2.016	0.50	0.167	-0.86	19.9	18.8	16.21	3.69	a
0821+394	1.216	2.59	1.234	-0.58	17.8	17.5	13.41	4.39	a
0821+447	0.893	2.26	0.715	-0.90	17.4	17.0	15.55	1.85	a
0827+378	0.914	5.17	1.859	-0.80	18.7	18.2	15.39	3.31	a
0829+425	1.056	0.82	0.401	-0.56	19.3	18.6	15.99	3.31	a
0836+426	0.595	1.12	0.488	-0.65	20.6	19.6	15.77	4.83	a
0849+424	0.978	1.31	0.415	-0.90	17.9	18.0	15.91	1.99	a
0859+470	1.462	2.81	2.148	-0.21	19.4	18.6	15.89	3.51	a
0906+430	0.670	11.90	3.913	-0.87	19.0	18.0	14.88	4.12	a
0913+391	1.250	1.65	1.199	-0.25	19.3	18.1	14.83	4.47	a
0918+381	1.108	2.45	0.624	-1.07	21.1	19.1	15.79	5.31	a
0922+422	1.750	0.97	0.209	-1.20	19.1	18.3	15.77	3.33	a
0922+425	1.879	1.15	0.242	-1.22	21.5	19.4	15.56	5.94	a
0923+392	0.698	3.33	2.968	-0.09	17.1	16.3	14.27	2.83	a
0926+388	1.630	0.50	0.124	-1.09	19.1	18.3	17.36	1.74	a
0945+408	1.252	2.45	1.277	-0.51	17.9	17.2	15.85	2.05	b
0951+408	0.783	10.92	0.247	-1.03	19.0	18.5	16.40	2.60	b
0953+398	1.179	0.50	0.296	-0.41	20.6	19.7	16.69	3.91	b
0955+387	1.405	1.42	0.348	-1.10	20.8	20.0	16.49	4.31	b
1007+417	0.613	4.10	1.493	-0.79	15.8	15.0	13.77	2.03	b
1015+383	0.380	0.64	0.213	-0.86	17.9	17.7	14.03	3.87	b
1020+400	1.250	1.77	1.103	-0.37	17.4	16.7	15.36	2.04	b
1030+415	1.120	1.02	0.589	-0.43	18.4	17.4	15.85	2.55	b
1105+392	0.781	2.31	0.760	-0.87	19.5	18.1	15.25	4.25	a
1109+437	1.680	4.77	1.184	-1.09	19.5	18.6	16.83	2.67	a
1111+408	0.734	0.92	2.479	-1.16	16.9	16.3	15.21	1.69	a
1128+385	1.735	0.52	0.793	0.33	19.5	18.6	15.78	3.72	a
1142+392	2.276	0.57	0.155	-1.02	18.8	18.0	16.21	2.59	a
1144+402	1.010	0.93	1.004	0.06	19.0	18.0	13.42	5.58	a
1148+387	1.303	1.83	0.550	-0.94	16.7	16.2	14.95	1.75	a
1148+477	0.867	2.29	0.500	-1.19	18.5	17.2	15.95	2.55	a
1203+384	0.838	0.67	0.191	-0.98	19.7	18.7	16.95	2.75	a
1206+439B	1.400	5.69	1.920	-0.85	18.1	16.7	14.88	3.22	a
1228+397	2.217	0.60	0.192	-0.89	18.5	17.9	15.53	2.97	b
1229+405	0.649	0.91	0.260	-0.98	19.8	19.0	15.86	3.94	b
1239+442B	0.610	1.21	0.373	-0.92	18.2	17.8	15.04	3.16	b
1242+410	0.811	2.01	1.460	-0.25	20.5	19.1	16.20	4.30	b
1247+450A	0.799	1.68	0.661	-0.73	17.7	17.2	15.29	2.41	b
1258+404	1.656	4.51	1.193	-1.04	19.3	19.0	15.99	3.31	a
1312+393	1.570	0.71	0.211	-0.95	21.2	20.0	16.54	4.66	a
1315+396	1.560	1.16	0.620	-0.49	18.4	17.6	16.32	2.08	a
1317+380	0.835	0.75	0.250	-0.86	19.6	19.1	16.83	2.77	a
1339+472	0.502	2.21	0.600	-1.02	19.8	19.7	15.48	4.32	a

TABLE 1. (continued)

B3 name	z	$S_{408,\mathrm{tot}}$ Jy	$S_{1460,\mathrm{tot}}$ Jy	α_{408}^{1460}	B	R	K	$B-K$	
1341+392	0.768	1.22	0.335	-1.01	21.5	19.9	16.10	5.40	a
1342+389A	1.533	0.86	0.213	-1.09	18.1	17.5	15.09	3.01	a
1343+386	1.844	1.52	0.823	-0.48	18.3	17.5	15.46	2.84	a
1355+380	1.561	0.60	0.192	-0.89	20.2	19.3	16.25	3.95	b

Notes to Table 1.

Last column gives the observing date: Feb 5th (a) and Feb 6th (b).

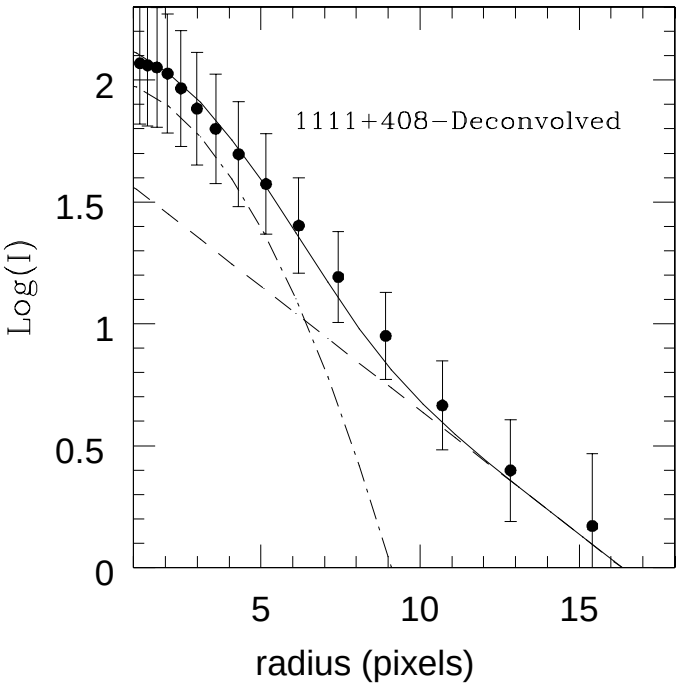
1111+408−Deconvolved
Log(I)
radius (pixels)
0
0.5
1
1.5
2
5
10
15

arXiv:astro-ph/9712220v1 17 Dec 1997

TABLE 2. Results of the fits to the surface brightness profiles of extended sources

	gauss	disk			$r^{1/4}$			King				
B3 name	rms	rms	$K_{\rm gal}$	$K_{\rm QSO}$	rms	$K_{\rm gal}$	$K_{\rm QSO}$	rms	$K_{\rm gal}$	$K_{\rm QSO}$	$\Delta K_{\rm gal}$	$\Delta K_{\rm QS}$
0704+384	2.25	0.76	17.0	15.5	0.71	17.0	15.5	0.31	16.7	15.6	0.3	0.1
0726+431	0.60	0.31	17.2	17.7	0.27	17.5	17.4	0.11	17.8	17.2	0.6	0.5
0739+397B	0.38	0.10	16.6	16.9	0.14	17.0	16.5	0.37	17.2	16.4	0.4	0.4
0740+380C	1.49	0.46	17.1	15.5	0.44	17.1	15.5	0.43	17.1	15.5	0.0	0.0
0756+406	0.46	0.21	16.5	17.9	0.26	16.5	17.9	0.17	17.1	16.8	0.6	1.1
0836+426	1.34	0.45	16.4	16.7	0.48	16.3	16.8	0.27	16.2	16.9	0.2	0.5
0849+424	0.28	0.09	17.5	16.2	0.10	17.5	16.2	0.07	17.2	16.3	0.3	0.1
0859+470	0.39	0.11	16.8	16.5	0.12	16.8	16.5	0.11	16.7	16.6	0.3	0.1
0906+430	1.40	0.36	16.1	15.3	0.50	···	14.9	0.48	15.8	15.5	0.3	0.2
0913+391	0.57	0.22	15.2	16.1	···	···	···	0.26	15.4	15.9	0.1	0.2
0918+381	0.71	0.35	16.0	17.7	0.41	16.1	17.2	0.68	17.3	16.1	0.1	0.5
0922+422	1.19	0.46	16.1	17.3	0.50	16.1	17.3	0.84	16.0	17.5	0.1	0.2
1111+408	1.15	0.32	16.3	15.7	0.36	16.1	15.8	1.07	···	15.2	0.2	0.1
1142+392	1.67	0.58	16.7	17.4	0.57	16.7	17.3	0.74	16.5	17.7	0.2	0.4
1315+396	0.24	0.09	16.6	17.8	0.23	17.9	16.6	0.14	17.0	17.1	0.4	0.7
1341+392	1.56	0.44	16.9	16.8	0.49	16.8	16.9	0.48	16.9	16.8	0.1	0.1

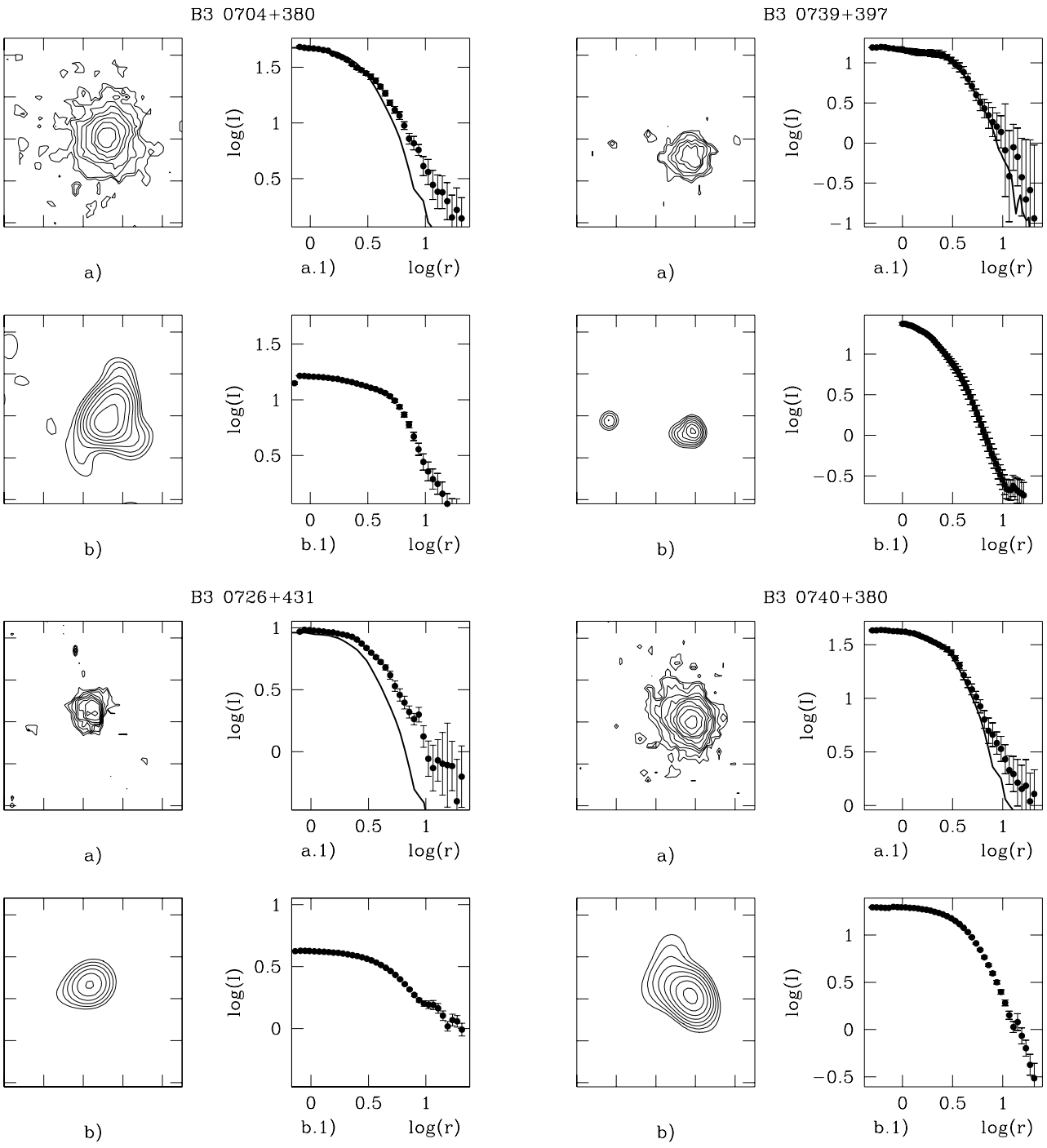
B3 0704+380
B3 0739+397
B3 0726+431
B3 0740+380
log(I)
log(r)
a)
a.1)
b)
b.1)

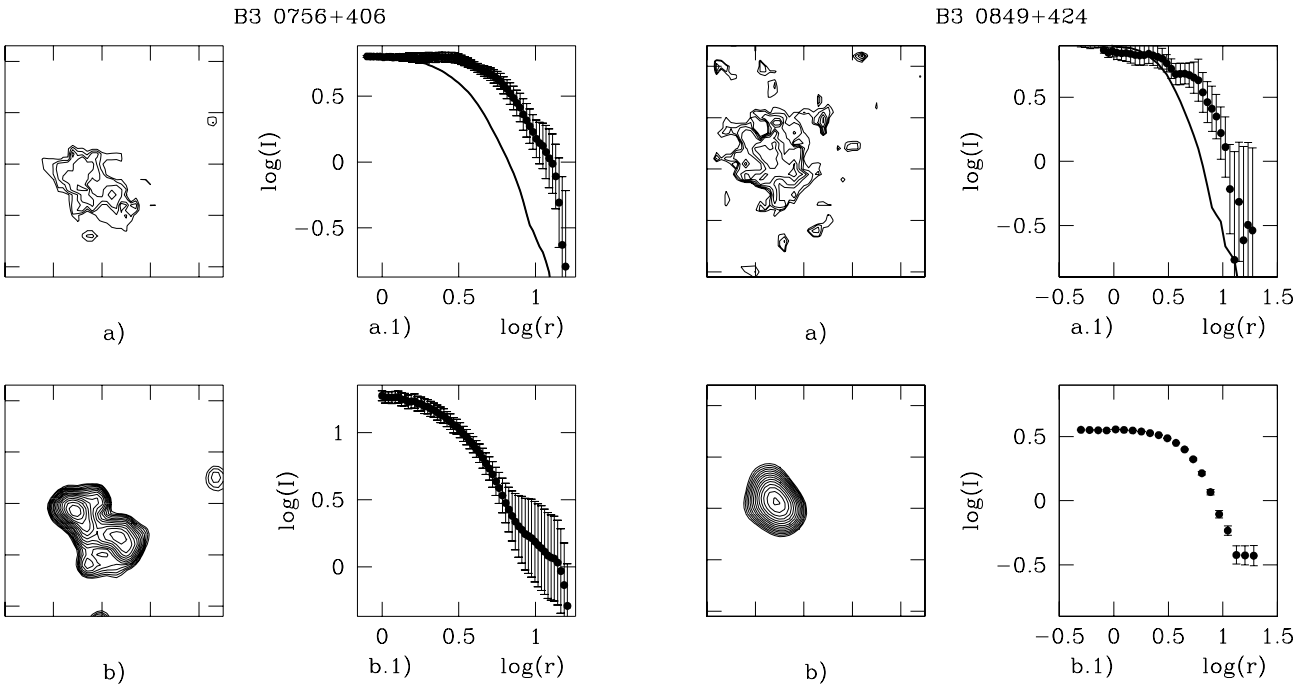
B3 0756+406
B3 0849+424
log(I)
log(r)
a)
a.1)
b)
b.1)

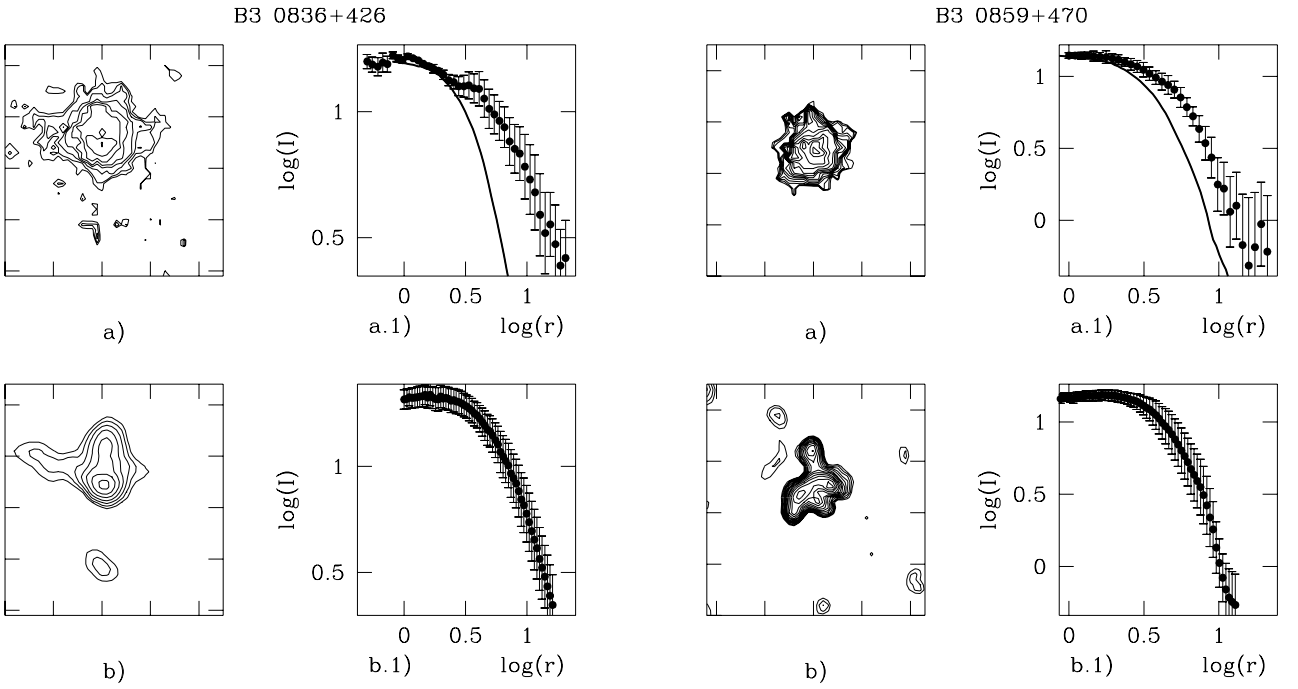
B3 0836+426
B3 0859+470
log(I)
log(r)
a)
a.1)
b)
b.1)

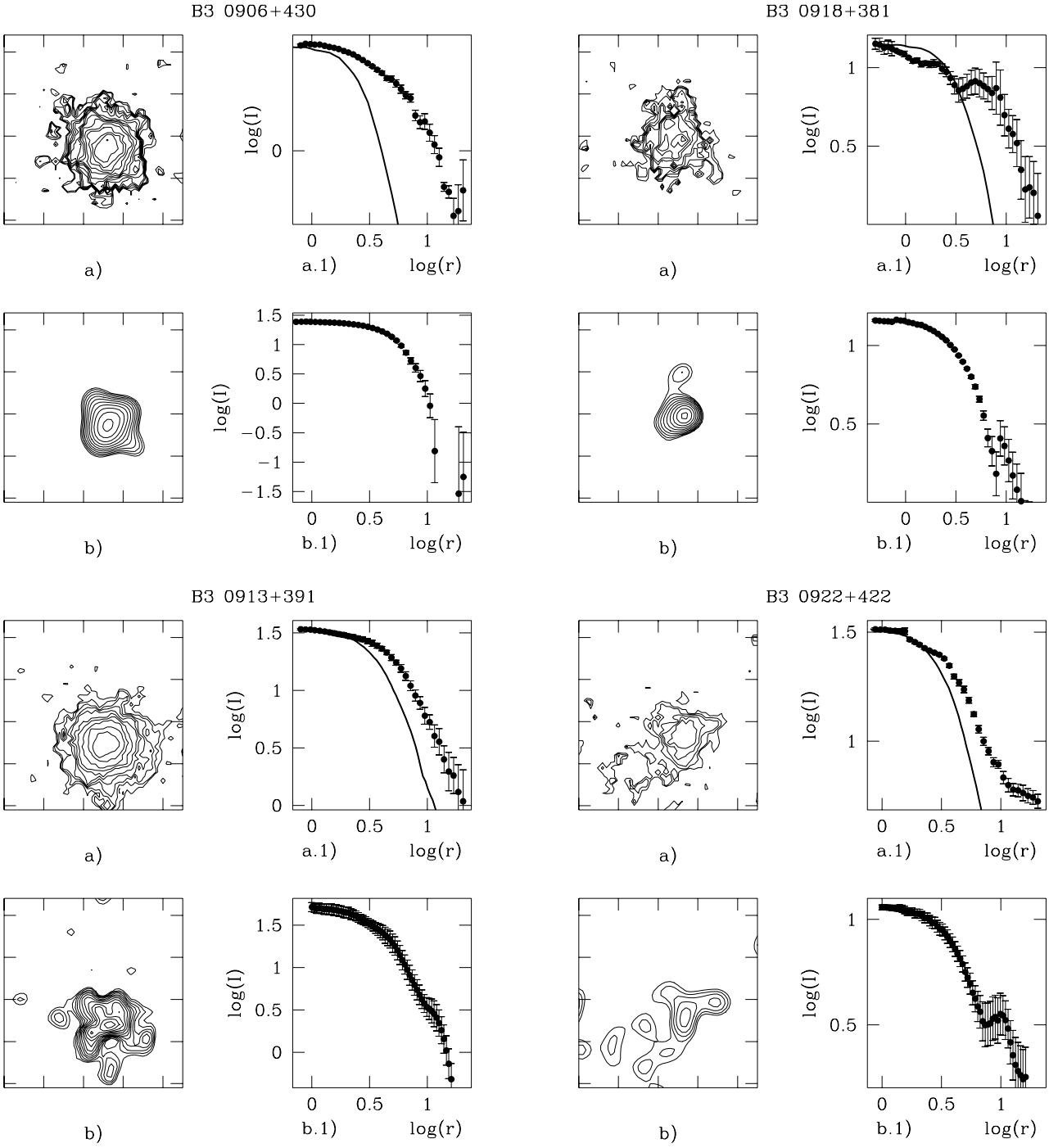
B3 0906+430
B3 0918+381
B3 0913+391
B3 0922+422
log(I)
log(r)
a)
a.1)
b)
b.1)

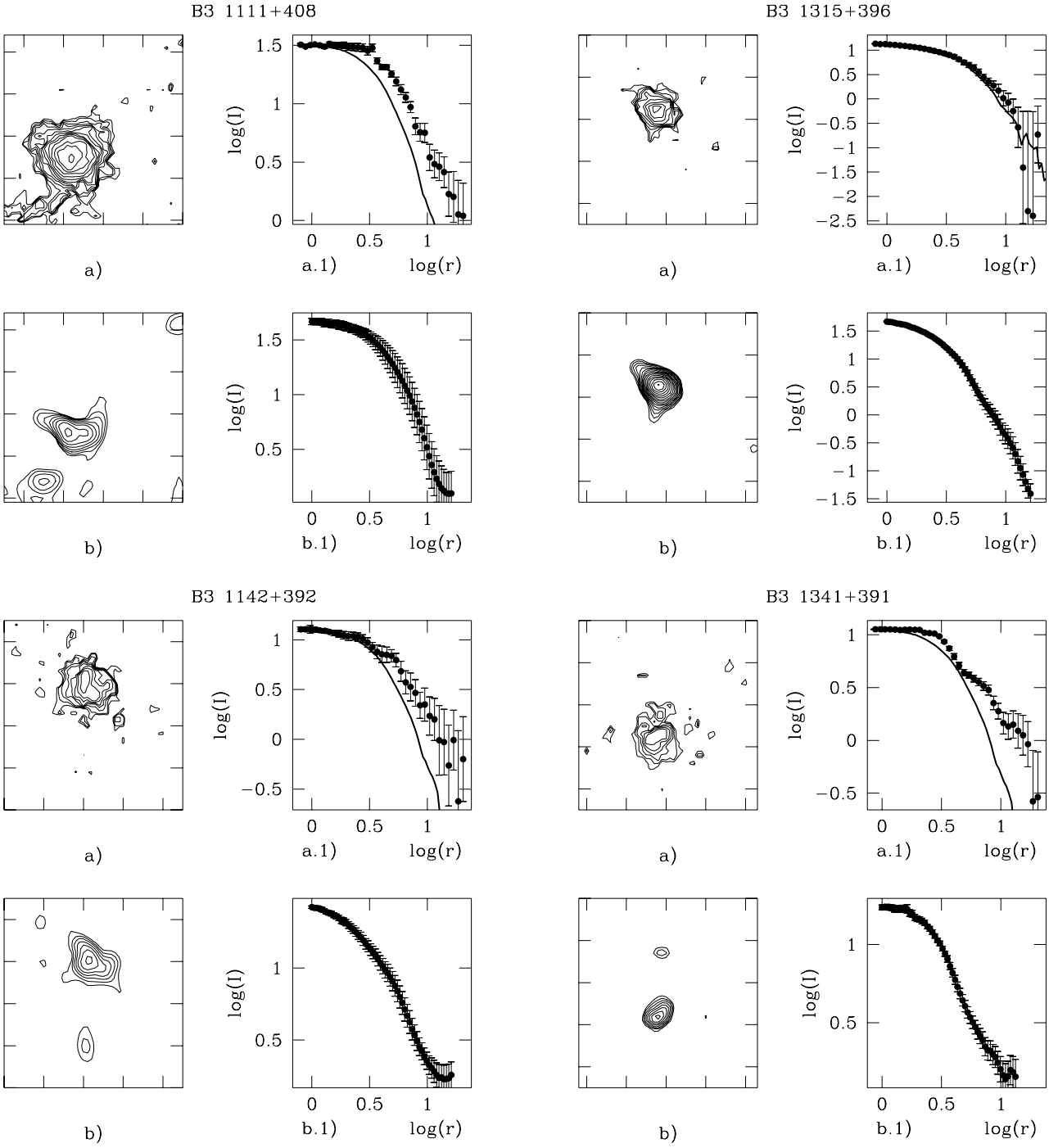
B3 1111+408
B3 1315+396
B3 1142+392
B3 1341+391
log(I)
log(r)
a)
a.1)
b)
b.1)

arXiv:astro-ph/9712220v1 17 Dec 1997

TABLE 3. K magnitudes of the host galaxies

B3 name	z	$K_{\rm gal}$	$\sigma(K_{\rm gal})$	$L_{\rm gal}/L_{\rm tot}$	k^a	e^a	$M_{\rm K,gal}$ [b]
0704+384	0.579	16.7	0.4	27%	-0.64	-0.46	-25.14
0726+431	1.072	17.8	0.6	37%	-0.91	-0.86	-24.83
0739+397B	1.700	16.6	0.4	57%	-0.69	-1.37	-26.85
0740+380C	1.063	17.1	0.4	18%	-0.91	-0.86	-25.51
0756+406	2.016	17.1	0.6	42%	-0.56	-1.74	-26.53
0836+426	0.595	16.2	0.3	65%	-0.64	-0.49	-25.67
0849+424	0.978	17.2	0.3	30%	-0.89	-0.78	-25.31
0859+470	1.462	16.8	0.3	43%	-0.80	-1.17	-26.38
0906+430	0.670	16.1	0.5	32%	-0.68	-0.52	-25.98
0913+391	1.250	15.2	0.2	69%	-0.90	-1.01	-27.66
0918+381	1.108	16.0	0.4	83%	-0.91	-0.87	-26.70
0922+422	1.750	16.1	0.5	75%	-0.66	-1.43	-27.39
1111+408	0.734	16.3	0.4	36%	-0.73	-0.59	-25.88
1142+392	2.276	16.7	0.6	63%	-0.46	-2.05	-27.01
1315+396	1.560	16.6	0.4	74%	-0.75	-1.28	-26.67
1341+392	0.768	16.9	0.4	47%	-0.76	-0.58	-25.36

[a] c-model, $\tau = 1$ Gyr, $z_{\rm for} = 10$.
[b] $k + e$ corrections applied.

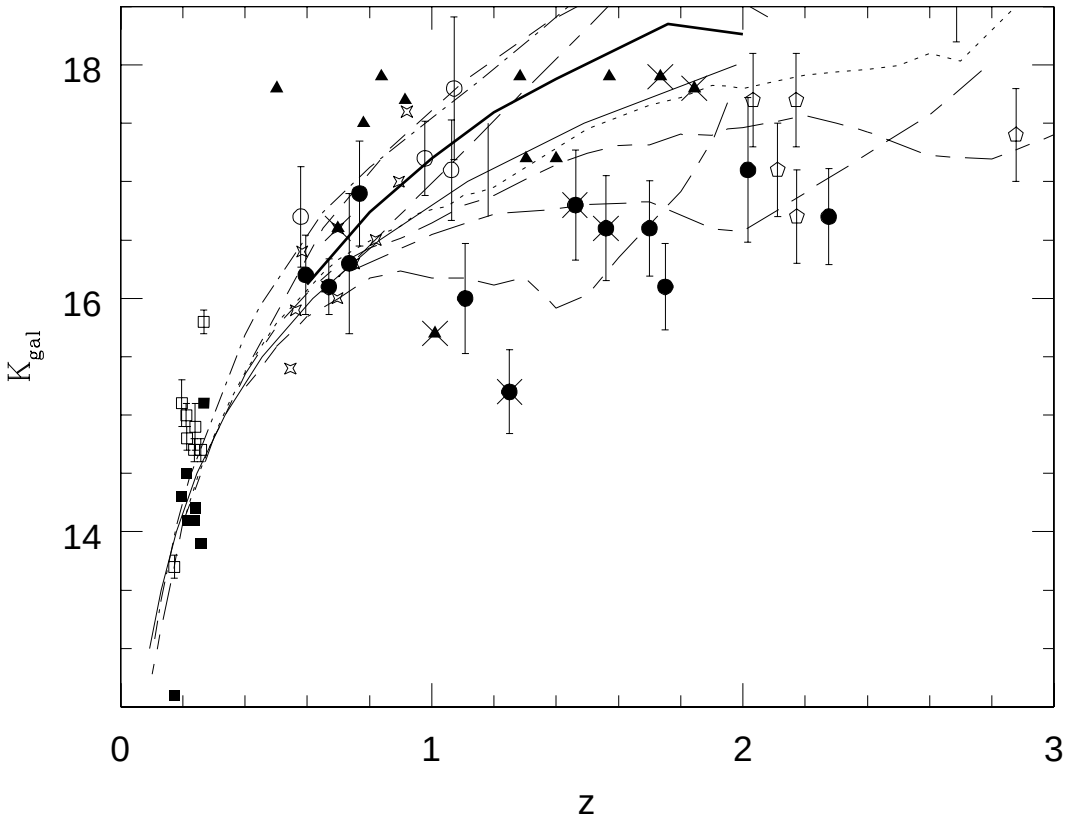
18
16
14
K_{gal}
0
1
2
3
z

arXiv:astro-ph/9712220v1 17 Dec 1997

TABLE 4. K magnitudes of the quasar nuclei

B3 name	z	$K_{\rm QSO}$	$\sigma(K_{\rm QSO})$	$M_{\rm K,QSO}$	
0701+392	1.283	16.47		-28.36	p
0704+384	0.579	15.6	0.3	-27.34	e
0726+431	1.072	17.2	0.5	-27.20	e
0739+397B	1.700	16.9	0.4	-28.61	e
0740+380C	1.063	15.5	0.4	-28.88	e
0756+406	2.016	16.8	1.1	-29.13	e
0827+378	0.914	15.39		-28.63	p
0836+426	0.595	16.9	0.6	-26.10	e
0849+424	0.978	16.3	0.1	-27.88	e
0859+470	1.462	16.5	0.1	-28.65	e
0906+430	0.670	15.3	0.4	-27.98	e
0913+391	1.250	16.1	0.3	-28.67	e
0918+381	1.108	17.7	0.6	-26.78	e
0922+422	1.750	17.3	0.5	-28.28	e
0923+392	0.698	14.27		-29.11	p
1105+392	0.781	15.25		-28.39	p
1111+408	0.734	15.7	0.3	-27.80	e
1128+385	1.735	15.78		-29.78	p
1142+392	2.276	17.3	0.7	-28.92	e
1144+402	1.010	13.42		-30.84	p
1148+387	1.303	14.95		-29.92	p
1203+384	0.838	16.95		-26.86	p
1206+439B	1.400	14.88		-30.16	p
1312+393	1.570	16.54		-28.78	p
1315+396	1.560	17.8	0.4	-27.50	e
1339+472	0.502	15.48		-27.12	p
1341+392	0.768	16.8	0.4	-26.80	e
1343+386	1.844	15.46		-30.25	p

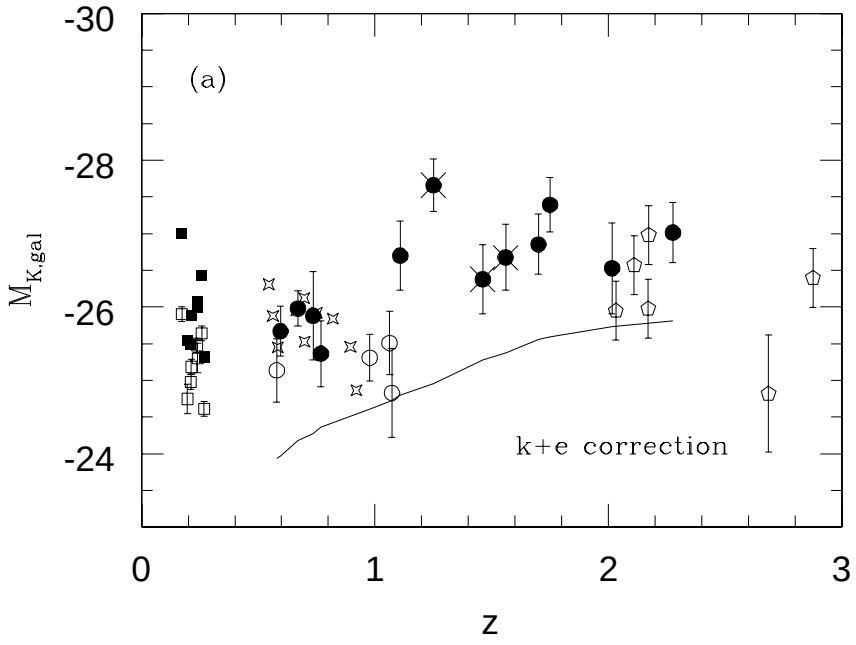
(a)
k+e correction
$M_{K,gal}$
z
-30
-28
-26
-24
0
1
2
3

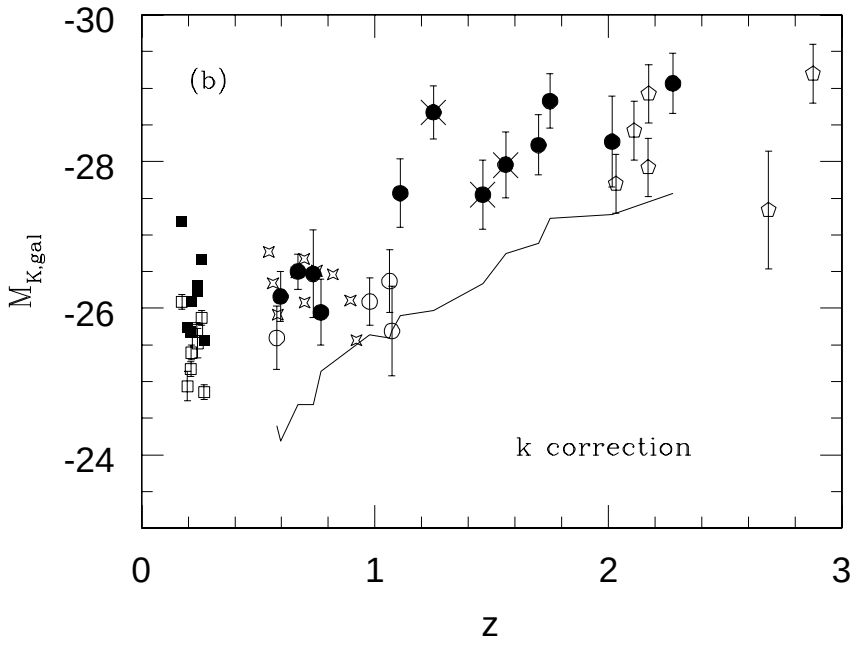
(b)
k correction
$M_{K,gal}$
z
-30
-28
-26
-24
0
1
2
3

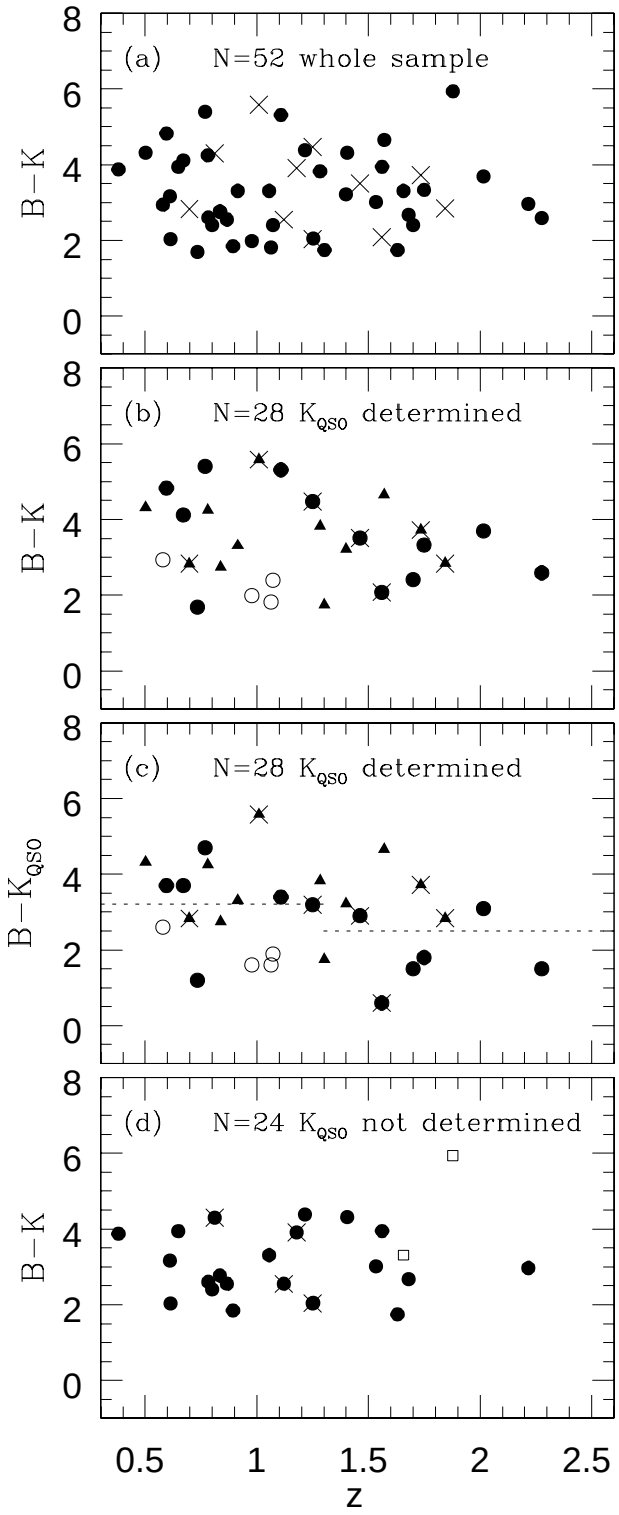
(a) N=52 whole sample
(b) N=28 K_{QSO} determined
(c) N=28 K_{QSO} determined
(d) N=24 K_{QSO} not determined
B−K
B−K_{QSO}
z
0
2
4
6
8
0.5
1
1.5
2
2.5

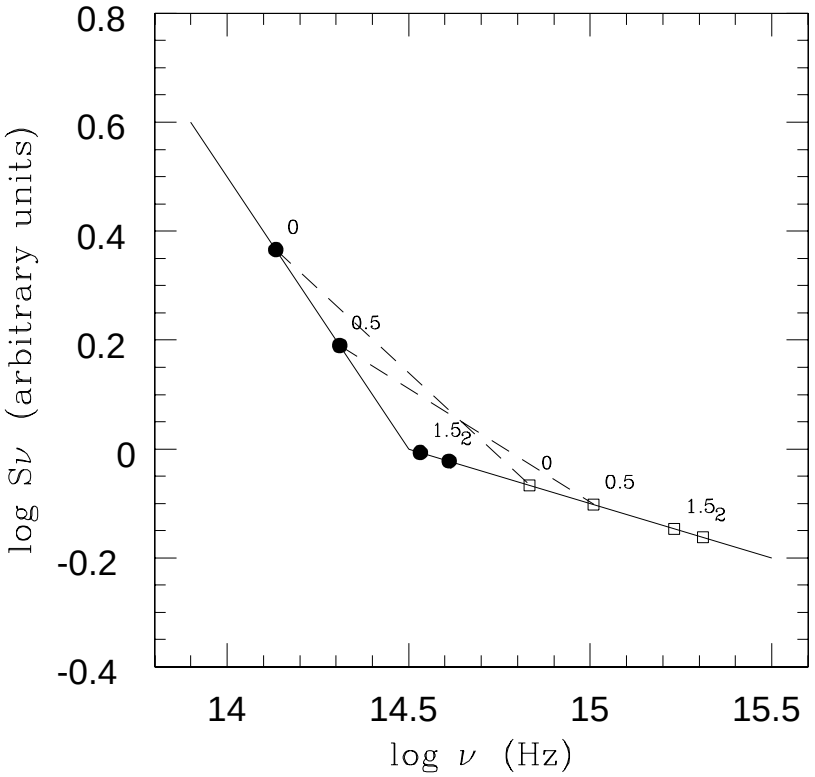
0.8
0.6
0.4
0.2
0
-0.2
-0.4
14
14.5
15
15.5
log Sν (arbitrary units)
log ν (Hz)
0
0.5
1.5
2
0
0.5
1.5
2

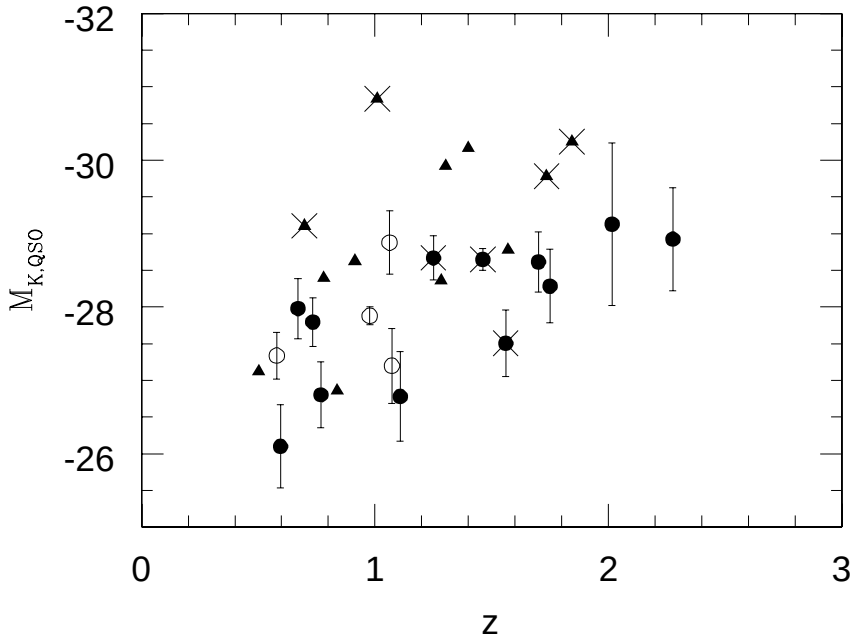
-32
-30
-28
-26
$M_{K,QSO}$
0
1
2
3
z

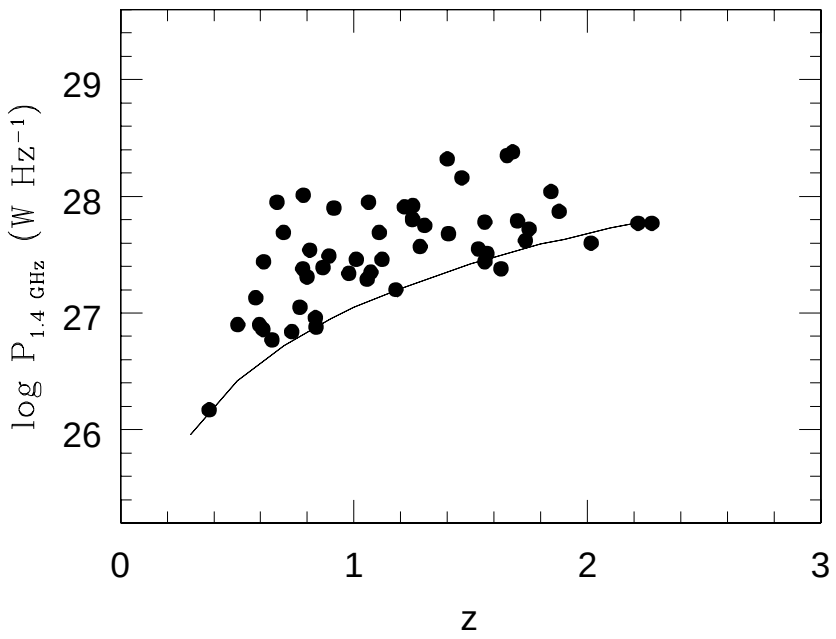
29
28
27
26
log P1.4 GHz (W Hz−1)
0
1
2
3
z

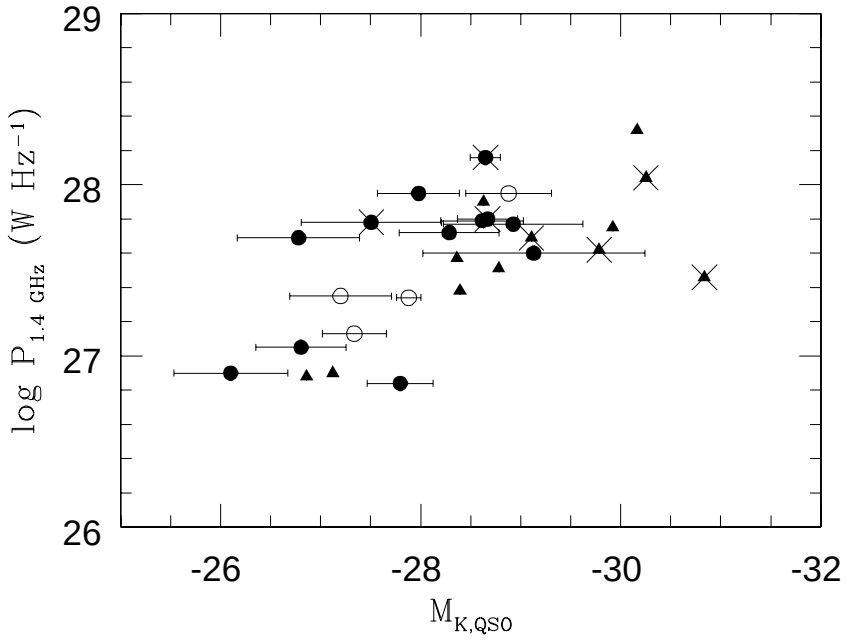
29
28
27
26
log P1.4 GHz (W Hz−1)
-26
-28
-30
-32
MK,QSO

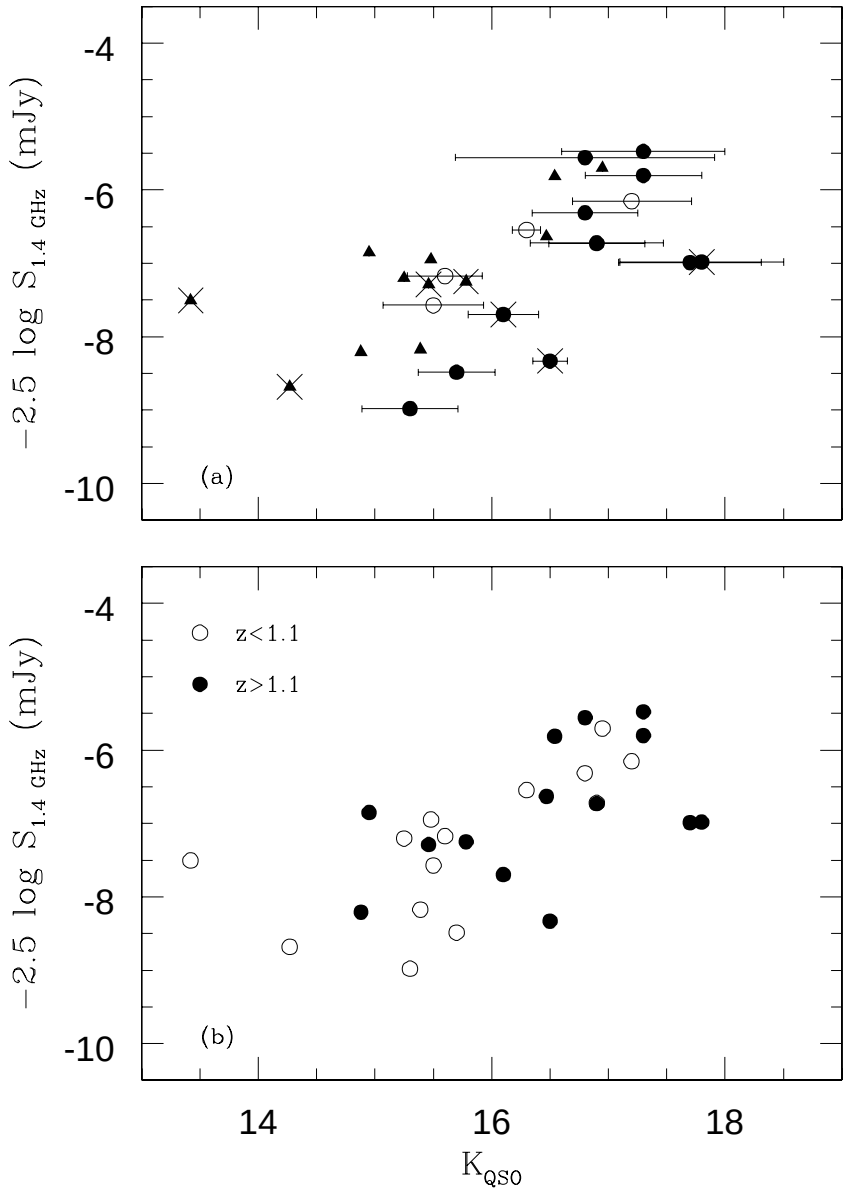
-4
-6
-8
-10
$-2.5 \log S_{1.4\ GHz}$ (mJy)
(a)
z<1.1
z>1.1
(b)
14
16
18
K_{QSO}

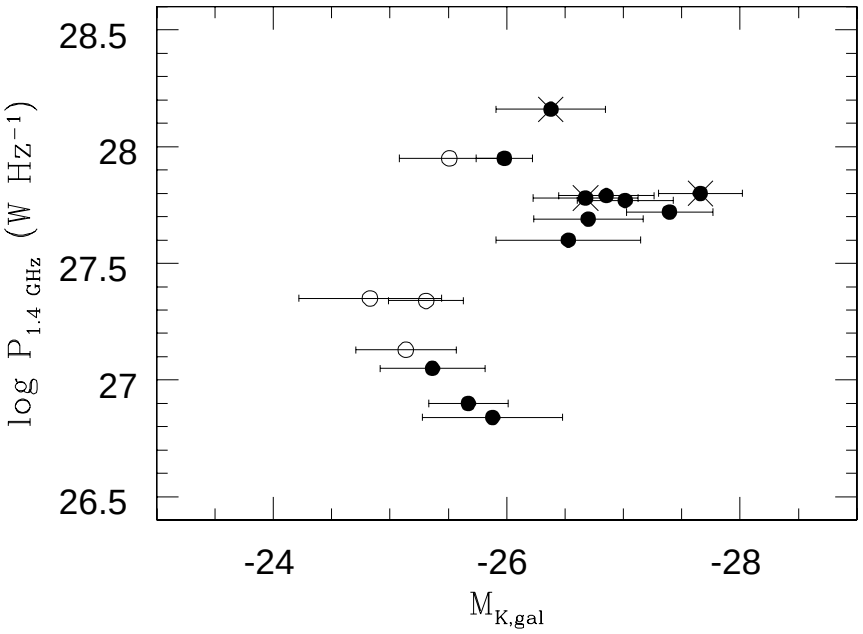
28.5
28
27.5
27
26.5
log P1.4 GHz (W Hz-1)
-24
-26
-28
MK,gal

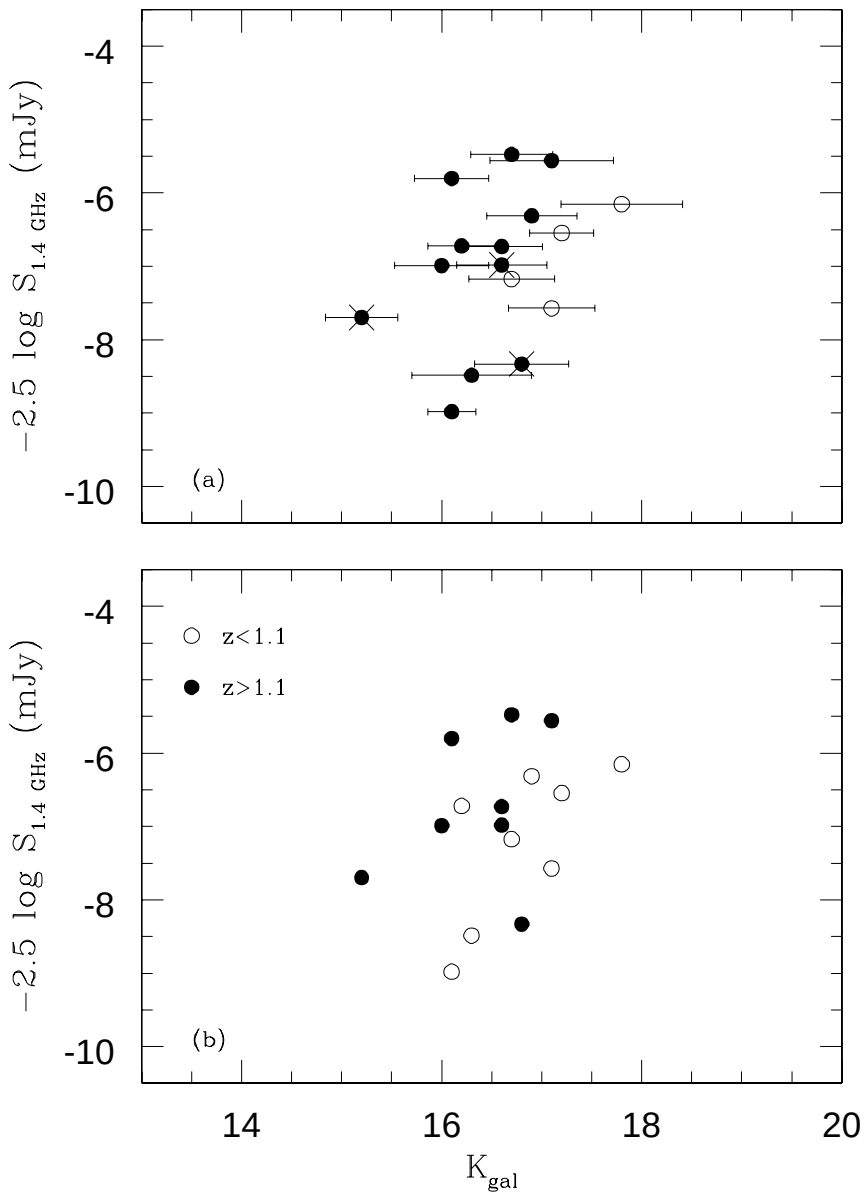
-4
-6
-8
-10
$-2.5 \log S_{1.4\ GHz}$ (mJy)
(a)
z<1.1
z>1.1
(b)
14
16
18
20
K_{gal}

arXiv:astro-ph/9712220v1 17 Dec 1997

K-band imaging of 52 B3-VLA quasars: Nucleus and host properties

R. Carballo, S.F. Sánchez

Instituto de Física de Cantabria (CSIC-Universidad de Cantabria) and Departamento de Física Moderna (Universidad de Cantabria). Facultad de Ciencias, 39005 Santander, Spain

Electronic mail: carballo@ifca.unican.es, sanchez@ifca.unican.es

J.I. González-Serrano

Instituto de Física de Cantabria (CSIC-Universidad de Cantabria). Facultad de Ciencias, 39005 Santander, Spain

Electronic mail: gserrano@ifca.unican.es

C.R. Benn

Isaac Newton Group. Apartado 321, 38780 Santa Cruz de la Palma, Spain

Electronic mail: crb@ing.iac.es

and

M. Vigotti

Istituto di Radioastronomia di Bologna, CNR, Via Gobetti 100, 40100 Bologna, Italy

Electronic mail: vigotti@astbo1.bo.cnr.it

Received _____; accepted _____

ABSTRACT

We present K-band imaging and photometry of a sample of 52 radio loud quasars (RQs) selected from the B3 survey with flux densities above 0.5 Jy at 408 MHz. The optical completeness of the sample is 90% and the quasars cover the redshift range 0.4 – 2.3. For $\sim$ 57% of the sources for which the quality of the images allowed a detailed morphological study (16/28) resolved extended emission was detected around the QSO, and its K flux was measured. Interpreting this "fuzz" as starlight emission from the host galaxy, its location on the $K - z$ plane at $z < 1$ is consistent with radio quasars being hosted by galaxies similar to radio galaxies (RGs) or giant ellipticals (gEs). At higher redshifts the detected host galaxies of RQs are more luminous than typical RGs and gEs, although some weak detections or upper limits are consistent with a similar fraction of RQs being hosted by galaxies with the expected luminosities for RGs or gEs.

The study of the $B-K$ colour distribution of the QSO nuclei, after removing the contribution of K emission from the host galaxy, confirm that these sources are not reddened by large amounts of dust, with an estimated extinction $A_{\rm V} < 1.0$ mag at $z \simeq 1$.

We found a significant correlation between radio power and nuclear infrared luminosity indicating a direct link between the radio synchrotron emission and the nuclear emission in K. This correlation is more tight for the steep-spectrum sources (99.97% significance). In addition, a trend is found between radio power and infrared luminosity of the host galaxy (or mass), in the sense that the most powerful quasars inhabit the most luminous galaxies. The similarity of this tendency with that found for powerful FR-II radio galaxies is consistent with the unification model for radio sources.

Subject headings: galaxies: active – galaxies: evolution – galaxies: photometry – infrared: galaxies – quasars: general

1. INTRODUCTION

The B3-VLA Sample (Vigotti et al. 1989) is a catalogue of 1050 radio sources selected at 408 MHz, consisting of five complete subsamples in the flux density ranges 0.1-0.2 Jy, 0.2-0.4 Jy 0.4-0.8 Jy, 0.8-1.6 Jy and $S_{408} > 1.6$ Jy, and all mapped at the VLA in A and C configurations at 1.46 GHz. From this catalogue Vigotti et al. (1997) obtained the B3-VLA Quasar Sample, consisting of 125 sources with an starlike counterpart in the POSS-I red plates with $R < 20$ mag and spectroscopically confirmed as quasars. The sample covers the redshift range $z = 0.3 - 2.8$, with median redshift $z = 1.16$, and radio powers $P_{1.4\ \mathrm{GHz}} \simeq 10^{27} - 10^{28}$ WHz^{-1} (the adopted cosmology in this work is $H_\circ = 50$ km s^{-1} Mpc^{-1} and $\Omega_\circ = 1$).

The flux distribution of the Quasar Sample is as follows: 30 quasars with 0.1 Jy $< S_{408} <$ 0.4 Jy, 31 quasars with 0.4 Jy $< S_{408} <$ 0.8 Jy and 64 quasars with $S_{408} > 0.8$ Jy. The optical incompleteness of the sample, i.e. the fraction of quasars fainter than the optical limit $R \simeq 20$ mag, depends on radio flux and is estimated to be around 6% for $S_{408} > 0.8$ Jy, 10% for $S_{408} > 0.6$ Jy and 30% for the flux bin 0.1-0.6 Jy (Vigotti et al. 1989, 1997; Benn et al. 1997, hereafter Paper I).

Being selected at a low frequency most of the quasars have steep spectrum. The most notable radio sample selected at low frequencies previous to the B3-VLA sample is the Third Cambridge Revised Radio Sample (3CR, Spinrad et al. 1985; Laing et al. 1983), with optical identifications and redshift measurements for all the sources. The 3CR sample has a limiting flux of 9 Jy at 178 MHz and the median redshift for the quasars is 0.7. The B3-VLA Quasar Sample thus allows the study of low frequency selected radio quasars (hereafter RQs) reaching lower luminosities and higher redshifts than the 3CR sample. A similar low-frequency selected sample is the Molonglo Reference Catalogue/1 Jansky survey (MRC/1Jy, McCarthy et al. 1996; Kapahi et al. 1996; Large et al. 1981), with a flux limit

of 0.95 Jy at 408 MHz and available optical identifications and redshifts for most of the sources. We have started an observing programme aimed at the study of the optical and near-infrared spectral energy distribution (hereafter SED) of the B3-VLA quasars and the nature of their host galaxies.

One of the aims of the study of the optical to near-infrared SED of the nucleus of these quasars was to determine the amount of reddening due to dust absorption. Being a radio-selected sample, it does not have in principle any bias against obscured objects. The question about the existence of obscured quasars and their number is crucial, since a large fraction of obscured QSOs, such as the one claimed by Webster et al. (1995), would imply profound revisions in well-established properties of QSOs derived from optical surveys, such as the quasar optical luminosity function and its evolution. The claim by Webster et al. (1995) of a large fraction of obscured quasars was based in the red $B-K$ colours they found in a sample of flat-spectrum PKS RQs, which they attribute to dust reddening. However, as noted by Rieke, Lebofsky & Wisniewski (1982) and Serjeant & Rawlings (1996), the red colours of flat-spectrum RQs could be due to enhanced synchrotron emission, which extends to the optical-infrared, due to relativistic beaming in a direction close to the line of sight. The B3-VLA Quasar Sample, being predominantly a steep-spectrum sample, is appropriate to determine the reddening using the unenhanced (not beamed) core flux. Baker & Hunstead (1995) and Baker (1997) infer from the large Balmer decrements in Molonglo lobe-dominated quasars extinctions up to $A_{\rm V} \simeq 3.7$, but considerably less extinction is implied by the small reddening of the continua; the maximum slope $\alpha_{\rm opt} \simeq -2.2$ (the spectral index α is defined as $S_\nu \propto \nu^\alpha$) corresponding to $A_{\rm V} \simeq 1.4$ mag, assuming intrinsic spectra $\alpha_{\rm opt} = -0.5$. The interpretation of the Balmer decrements in the broad line regions of quasars is not straightforward, as they depend on other effects apart from dust reddening, such as radiative-transfer and collisional-excitation effects (Osterbrock 1989, Baker et al. 1994). Furthermore it is not clear that the same extinction applies to the broad emission

lines and the continuum.

Detailed studies of the host galaxies of active galactic nuclei (AGN) are necessary to determine what kind of galaxies are able to "feed" an active nucleus, and to understand this phenomenon. The comparison between the properties of the host galaxies of different classes of AGN is crucial to explain the differences in nuclear activity. In particular the comparison between the host properties of RQs and RGs provides an effective test to the Unified Schemes for extragalactic radio sources (see Antonucci 1993 for a review).

The general picture that has emerged from the study of RQ hosts in the redshift ranges $z = 0.2 - 1.0$ (e.g. Smith et al. 1986; Hutchings 1987; Véron-Cetty & Woltjer 1990; Dunlop et al. 1993, and their updated work in Taylor et al. 1996; Disney et al. 1995; Rönnback et al. 1996) and $z = 2 - 3$ (Lehnert et al. 1992, hereafter L92) is that these galaxies have an elliptical morphological type (Véron-Cetty & Woltjer; Disney et al.; Rönnback et al.; Taylor et al., hereafter T96) and large sizes and K-band luminosities ($M_{\rm K} \simeq -26$; L92, T96), similar to those of giant ellipticals, which is also the type of hosts harbouring RGs (Lilly et al. 1985; Lilly 1989; Rigler et al. 1992; Best et al. 1997). The host galaxies of RQs frequently exhibit morphological peculiarities in the form of tails visible from the optical to the infrared, and a high incidence of companions, suggesting interactions or merging processes in these galaxies (Hutchings; Smith et al.; Disney et al.; Hutchings & Neff 1997). Tails seen in the infrared indicate in fact morphological peculiarities in old stars, not related to nuclear radiation or star formation. This characteristic is also shared with RGs, for which a large fraction (50-75 %) shows evidence of ongoing or past interaction/merging processes (Heckman et al. 1986 for FRII powerful RGs; González-Serrano, Carballo & Pérez-Fournon, 1993 for FRI low-luminosity RGs). Recently, optical structure coincident with radio structure and interpreted as optical synchrotron was detected in three 3C RQ hosts (Ridgway & Stockton 1997). The flux contribution of the synchrotron emission

relative to the host galaxy is estimated to be around 10% in the optical and lower than this value in the infrared.

The SED in the optical-infrared of several RQ hosts studied by L92 and Rönnback et al. (1996) is bluer than expected for elliptical galaxies, although this was the type of galaxies implied by the luminosity profiles and the $K-z$ relation. This result was also found for RGs (Lilly & Longair 1982, 1984), which show a rather wide range of optical-to-near-infrared colours. The wide range of colours and the tight $K-z$ relation for RGs in the redshift range $0.5 < z < 2.0$ were explained by Lilly (1989, see also Rigler et al. 1992 and Lilly 1993) assuming a two-component model comprising the cool and old red giant stars evolved from the stellar population dominating the galaxy mass, contributing more than 80% of the K emission, and a young population of stars, i.e. a "burst of star formation" which explains the excess emission in the optical and ultraviolet. Detailed observations of the morphology of the optical continuum in RGs (rest-frame ultraviolet) revealed that in most of the blue RGs at $z \gtrsim 0.8$ this emission is aligned with the radio axis, although the optical structure is not spatially coincident with the radio structure (McCarthy et al. 1987; Chambers, Miley & van Breugel 1987). The so-called "alignment effect" is one of the most intringuing properties of RGs and the two most compelling explanations proposed have been scattered light from an anisotropically radiating nuclear source and star formation triggered by the radio jet (see McCarthy 1993 for a review). Both mechanisms may operate, although the dominant process appears to be scattering of nuclear light at $z \sim 1$ and induced star formations at $z > 3$ (Cimatti et al. 1997; Dey et al. 1997 and references in these papers). The alignment is weaker for the infrared emission of RGs, which is more symmetrical and nuclear concentrated, as expected for an old stellar population (Rigler et al. 1992). These authors found that in typical 3C RGs at $z \sim 1$ the active aligned component contributes about 10% of the infrared light. The infrared light profiles of the $z \simeq 1$ RGs with only small blue components are in fact well fitted by a de Vaucouleurs law (Rigler & Lilly 1994;

Best et al. 1997), although presenting in some cases excesses at large radii similar to those present in cDs (Best et al. 1997).

L92 and Rönnback et al. (1996) suggest these same arguments of recent star formation events or some contribution of scattered QSO light at the higher frequencies to explain the blue colours of the RQ hosts in their studies. We note that the work by L92 was biased towards the selection of blue hosts, since L92 RQs were selected for the presence of extended UV-optical emission, and in fact all contain extended Lyα emission (Heckman et al. 1991). The sample used by Rönnback et al. (1996) for their optical study of RQ hosts is not well defined. The B3-VLA Quasar Sample is appropriate to perform a systematic study of RQ hosts using a well-defined sample, not biased in principle towards the selection of blue objects. If the B3-VLA quasars are hosted by large luminous galaxies similar to those found by L92 and T96 they would be detectable in standard infrared images obtained in 2-4 m telescopes.

In this work we present near-infrared imaging in the K band of a representative group of 52 quasars in the B3-VLA Quasar Sample. We selected the 47 quasars in this sample with $S_{408} > 0.6$ Jy and right ascensions in the range $7^{\rm h} - 14^{\rm h}$, so that they could be observed in winter time, plus seven quasars with 0.5 Jy $< S_{408} <$ 0.6 Jy and similar right ascensions. Two of the sources were excluded from the study, since the identification of the quasar on the K images was ambiguous. The optical completeness of this sample is estimated to be around 90% (Paper I and references therein). The quasars cover the redshift range $z = 0.4 - 2.3$ and the mean redshift is $z = 1.18$. This near-infrared database allowed us to address three questions:

(i) Loci of the 16 detected RQ hosts on the $K - z$ diagram and interpretation in terms of standard galaxy evolution models.

(ii) Analysis of the $B - K$ colours of quasar nuclei after fuzz subtraction to impose limits

on the relative amounts of obscuration in this sample. In Paper I we performed this study using the total quasar K magnitudes, uncorrected from the host galaxy emission.

(iii) Infrared luminosities of host and quasar nuclei and their relation with radio power.

The organization of the paper is as follows. The observations, standard data reduction and K photometry of the total quasar light is presented in Sect. 2. In Sect. 3 we describe the technique used to separate the nucleus and host galaxy component of the quasars and give the resulting magnitudes of each component for the cases where both were detected. The issues (i), (ii), and (iii) above are discussed in Sects. 4-6 and the summary and conclusions are presented in Sect. 7.

2. OBSERVATIONS AND DATA REDUCTION

Near-infrared images of the 54 quasars were obtained on February the 5th and 6th 1996 using the 256×256 InSb infrared camera WHIRCAM at the Nasmyth focus of the 4.2m WHT on La Palma (Spain). The K_s filter was used and the pixel scale was set to 0.27 arcsec pixel^{-1}, corresponding to a field of view of $\sim 1' \times 1'$. The average seeing was ~ 1.9 arcsec and ~ 1.5 arcsec during the first and second nights, respectively. The $K_{\rm s}$ filter covers the wavelength range from 1.99 to 2.32 μm, with $\lambda_{\rm eff}$=2.16 μm. This filter is very similar to Johnson K, and hereafter we will refer to it as K.

In order to avoid saturation due to atmospheric emission in the infrared and obtain a high quality flat-field, the following observing procedure was used. For each source, short unregistered exposures were taken and the average image was registered. Five averaged images were obtained at five different positions on the CCD, one near the centre and the rest at symmetric directions at 9 arcsec offset relative to the first one. For the targets we

obtained 12 unregistered 10 s images per position and for the photometric standards 5 frames of 4 s per position. Care was taken that the sources did not fall on a dead column near the left side of the chip. A dark frame was obtained for every sequence of 5 registered images in order to correct for the dark current.

The data were reduced using standard tasks in the IRAF package. First, from each of the five registered images we subtracted the corresponding dark frame. A flat-field frame was obtained for each object using the average of the images obtained at the five different positions. This average was made clipping out the highest intensity in each pixel in order to remove the contribution from sources and cosmic-ray events. Each of the five images in the sequence was then corrected using this flat-field, and the final image was obtained as the average of the 5 flat-fielded images shifted to a common central position. The total exposure time of the final target frames was of 600 s.

All the images were obtained in good photometric conditions. Flux calibration for each night was carried out using UKIRT standard stars from the WHIRCAM User's Guide. Photometric calibration was better than 0.1 mag. The surface brightness level reached in the images is $\mu_K \simeq 22.6$ mag arcsec^{-2} and the 3σ limiting magnitude for point sources is $K \simeq 19$ mag.

All the quasars were detected on the images. For two objects (0937+391 and 1256+392) two possible counterparts were detected on the K images, both consistent with the optical/radio position, and it was impossible to tell which one was the right counterpart.

K magnitudes of the detected quasars were measured on the images using circular apertures centred at the emission peak. Aperture diameters ranged from 5.5 to 12 arcsec depending on the seeing, collecting $\sim 100\%$ of the light. Typical K magnitude errors are around ± 0.1 magnitudes. The K magnitudes are listed in Table 1, along with some optical and radio information about the quasars. The radio data, from Vigotti *et al.* (1989),

include the total flux density at 408 MHz and 1460 MHz, and the spectral index α_{408}^{1460}. The redshifts were taken from Vigotti et al. (1997). The B and R optical magnitudes in Table 1 were taken from the catalogue of objects on the POSS-I blue and red plates generated by the Automatic Plate-measuring Machine (APM) in Cambridge (Irwin 1992), and were corrected from Galactic extinction. The distribution of B and K magnitudes versus redshift of the B3-VLA quasars is shown in Figure 1. Crosses correspond to flat-spectrum sources, defined by $\alpha_{408}^{1460} > -0.5$.

3. ANALYSIS OF THE DATA

The main problem for the detection and photometry of quasar host galaxies is that the active nucleus dominates the quasar light in a large range of wavelengths, making difficult the substraction of the QSO from the image. As noted by Dunlop et al. (1993), at wavelengths around 1 μm, the SED of a normal galaxy has a maximum whereas that the SED of an active nucleus has a minimum (Sanders et al. 1989; Elvis et al. 1994). Therefore this is the best wavelength range to detect galaxy hosts, where the ratio of the nuclear to host galaxy emission is minimum. See Fig. 1 of McLeod & Rieke (1995) for the comparison between the SED of a typical galaxy and that of an active nucleus. At the mean redshift of the B3-VLA quasars of our study, $z = 1.18$, this rest-frame wavelength corresponds precisely to the K band. Another advantage in the use of the near infrared, compared to the optical, is that the galaxy infrared emission arises from the old stellar population, related to the galaxy mass. In fact some quasars show optical extended emission which is originated by transient phenomena in the gas, through its interaction with the active nucleus (Heckman et al. 1991).

In this work the quasar images were analysed using the following procedure. First surface brightness profiles were obtained from the deconvolved images. Then these profiles

were fitted with a two-component model describing the nuclear source and the galaxy. In fact the analysis assumes, as working hypothesis, that any detected extended emission component at K is stellar light from the host galaxy, and hence we used galaxy models to describe the extended emission. The contribution of extended emission in the K band due to an aligned component similar to that in RGs or beamed optical synchrotron emission is expected to be lower than 10% (Rigler et al. 1992; Ridgway & Stockton 1997). A fraction of nebulosities around quasars show strong UV/optical emission lines (Boroson & Oke 1984; Boroson, Persson & Oke 1985; Stockton & Mackenty 1987) which may reach equivalent widths of ~ 500Å but typically ~ 100Å. In the K filter we may have contribution of Hα emission from the fuzz for the three objects in the redshift range $2 < z < 2.3$, but from these equivalent widths we estimate a maximum contribution to the K flux of the fuzz around 15%, which is the fraction for the nebulosities with the strongest emission lines.

Due to some technical failure all the second night images are slightly out of focus, preventing the detailed analysis needed for the detection of the host galaxies. For this reason we restricted the search for host galaxies to the first night images (38 quasars). This problem with the second night images does not affect the quasar aperture K magnitudes presented in Table 1.

3.1. Point spread function (PSF) and image deconvolution

Atmospheric and instrumental point spread function has important effects not only on the spatial resolution but also on the observed surface brightness profiles of galaxies (Capaccioli & de Vaucouleurs 1983; Bailey & Sparks 1983) affecting mainly the central regions. The effect is specially strong when the galaxy has a bright point-like nucleus. As we are interested in measuring host galaxy fluxes, deconvolution allows us, not only a better separation of the nuclear component, but also a more accurate determination of galaxy and

nuclear fluxes.

Due to the small field of view of the images, $1' \times 1'$, only a few objects have stars in the frame, and in most cases, these are faint. We selected the four brightest field stars, distributed evenly through the first night, to built a normalized PSF. The FWHM of the PSF is 1.9 arcsec and it represents the average seeing of the night, which had variations of ± 0.3 arcsec (1 pixel). We used the Lucy-Richardson algorithm (Lucy 1974; Richardson 1972) and this PSF to deconvolve the images. Because of seeing variations and scarcity of good field stars this is not an ideal PSF for the whole night data. With a perfect PSF determination and infinite signal-to-noise data, the deconvolution process would produce a narrow ($\sim$ 1 pixel width) point source surrounded by some diffuse emission if this was present. However, it has been shown that there is a resolution limit due to photon noise which prevents the deconvolved PSF of being of zero FWHM (Lucy 1992). In our data, with moderate signal-to-noise and using an average FWHM, the mean FWHM of the stars after deconvolution is 1.3 ± 0.3 arcsec, with the dispersion reflecting the seeing variations and the intrinsic dispersion from the deconvolution process itself. It is important to stress that although there is not a large gain in spatial resolution, the deconvolution technique allows a better determination of the nuclear and extended fluxes.

3.2. Surface brightness profile fitting

Surface brightness profiles have been obtained for the deconvolved quasar images using the techniques discussed in Jedrzejewski (1987). In brief, given an initial value for the centroid of the object, the light distribution is sampled along a first-guess elliptical isophote. This produces a one-dimensional intensity distribution as a function of the eccentric anomaly. This distribution is then analyzed as a harmonic expansion in a Fourier series and finally, the parameters of the isophote (position angle, ellipticity) are estimated by a

least-squares fit. This procedure is repeated by increasing the semimajor axis of the ellipses until the sky background level is reached. The final product consists of semimajor-axis profiles of intensity, ellipticity and position angle. The resulting brightness profiles were fitted using an interactive least-square method. Four different models were used: (i) gaussian function; (ii) gaussian + King profile; (iii) gaussian + $r^{1/4}$ law; (iv) gaussian + exponential profile. The results of the analysis for the stars in the images showed that a gaussian function is the best representation of the PSF.

The original images of some of the quasars (10) were very noisy or they had (or could have) problems of bad tracking or a slight out-of-focus and we did not try to deconvolve them, although two of them (0922+425 and 1258+404) showed structure that could be real. The structure could have arisen because the host is part of a galaxy system, has multiple nuclei, or gravitational lensing produces several images of the quasar. We did not obtained the surface brightness profile of these 10 sources.

For the fitted surface brightness profiles each best fit provided us with two or four parameters: two for the central point source and two for the extended component if this was used. For the cases where we fitted a gaussian plus an extended component the QSO magnitudes ($K_{\rm QSO}$) were obtained directly from the model and the host magnitudes ($K_{\rm gal}$) were obtained from the difference between the total aperture flux (K magnitudes in Table 1) and the QSO flux from the model.

In order to set the reliability of the method we have applied the whole procedure (deconvolution, determination of the surface brightness profile and profile fitting) to 12 stars on the frames. This test is useful to quantify the effect of using an average PSF. In addition, the deconvolution algorithm could enhance the wings of bright sources, since the noise in the outer parts is high, and spurious detections of extended emission around point sources could arise because of this effect. Although for some of the stars a two-component model

gave a good fit, the extended component never contributed more than 12% to the total flux. This fraction corresponds to $K_{\rm gal} \sim 17.9$ mag for the average magnitude $K = 15.6$ of the quasars in the sample. This magnitude is approximately similar to the 3σ limiting magnitude of an extended source of size of ~ 10 arcsec, which is the typical size over which the fits were obtained. We used this magnitude, $K = 17.9$, as an absolute upper limit for the reliability of the detection of an extended component. For the quasars brighter than 15.6 the limit of 12% fixes a lower limiting magnitude for galaxy detection, corresponding to $K_{\rm gal} = 16.3$ for the brightest quasars with $K = 14$. A fractional contribution from the galaxy of 12% gives only a correction of 0.14 mag to the quasar K magnitude.

For twelve quasars a pure gaussian model produced a good fit giving small rms (less than 0.1 mag and typically 10^{-3} mag), and those were classified as point sources. These quasars are 0701+392, 0827+378, 0923+392, 1105+392, 1128+385, 1144+402, 1148+387, 1203+384, 1206+439B, 1312+393, 1339+472 and 1343+386. For the remaining 16 objects we found much larger residuals, clearly deviating from point sources, and their profiles were therefore fitted using models (ii), (iii) and (iv) explained above. Figure 2 shows an example of a fit with a $r^{1/4}$ galaxy model. For all of these cases the residuals for two or the three two-component models were smaller than the residuals for the gaussian fit, and the rms values for these fits were roughly similar. For this reason we could not determine from our data the galaxy type we were detecting. The fact that two or three different acceptable models give similar residuals is basically due to the rather low signal-to-noise ratio at the wings of the quasars.

3.3. Results. Apparent magnitudes of the quasar hosts galaxies

Table 2 shows the final results of the fitting procedure for the 16 quasars with a detected extended component[1]. Empty entries in the table correspond to one poor fit and two fits in which the fractional contribution of the galaxy was lower than 12% (in these two cases also $K_{\rm gal} > 17.9$. The table lists the residuals (rms in mags) and the parameters $K_{\rm gal}$ and $K_{\rm QSO}$ for these models, along with the residuals for the gaussian model for comparison. The two last columns of Table 2 give the maximum dispersion in $K_{\rm gal}$ and $K_{\rm QSO}$ between the different acceptable models for each source (excluding the two-component models giving rms similar to a pure gaussian model: King model for 0739+397, 0918+381 and 1111+408, and $r^{1/4}$ model for 1315+396). The average dispersion between the galaxy magnitudes derived from the acceptable models is 0.25 mag, the median is also 0.25 mag and the larger discrepancy is 0.6 mag. For $K_{\rm QSO}$ the average dispersion is 0.3 mag, the median is 0.2 mag and the largest discrepancy is 1.1 mag, for 0756+406.

There is in general a good agreement between the values of $K_{\rm QSO}$ and $K_{\rm gal}$ obtained for the different acceptable models. The similarity of $K_{\rm gal}$ for these models is a natural consequence of the way it is measured, subtracting from the total light the QSO contribution obtained from the model, which is roughly similar for the different acceptable models. The average dispersion of $K_{\rm QSO}$ and $K_{\rm gal}$ for the different acceptable models, of typically 0.3 mag, is similar to the average rms of the acceptable models, which is about 0.35 mag.

For the discussion on the next sections we have adopted as $K_{\rm QSO}$ and $K_{\rm gal}$ the values for the model with the minimum rms. The error in the apparent magnitude of each

[1]Four of these quasars were not considered as extended in Paper I, where we used a more restrictive criterion for host galaxy detection, i.e. a galaxy contribution higher than 30% and $K_{\rm gal} < 17.2$. These sources are 0704+384, 0726+431, 0740+380C and 0849+424.

component has to be obtained from the quoted rms of the fit and the dispersion due to the selection of one particular model, since for all cases there are at least two acceptable models, with roughly similar rms. Considering these errors in quadrature, the average error for the apparent magnitudes of the host galaxies is $\sigma(K_{\rm gal}) = 0.4 \pm 0.1$, and for the QSOs, $\sigma(K_{\rm QSO}) = 0.4 \pm 0.2$ (excluding the large error of 0756+406 from the average). The errors for these parameters correspond to the data dispersion.

We have obtained images of the galaxies subtracting the fitted point-like sources (obtained from the minimum rms model) from the deconvolved images. These images were then convolved with the original PSF so that they could be compared with the original quasar images, and we call them the 'restored' images. Figure 3 shows, for each object, contour plots of the original quasar image and the 'restored' host-galaxy image, and their corresponding surface brightness profiles, obtained as explained in Sect. 3.3 . The solid line on the brightness profile of the quasar shows the PSF profile rescaled to the quasar peak flux.

For 8 of the extended objects some morphological distorsions or peculiarities are apparent in both the original quasar images and the restored galaxy images. These are radial elongations, tails, distorsions, etc. However, since the signal-to-noise of these features is rather low we should take them with caution. Other sources (extended or not) have nearby objects in the field, but these are faint and we cannot confirm or reject their association with the radio source. All these possible companion objects were carefully masked before the surface photometry analysis was performed, and therefore they do not contaminate the surface brightness profiles.

4. K-z RELATION OF HOST GALAXIES

The apparent K magnitudes of the sixteen detected B3-VLA quasar hosts are listed in Table 3, along with their errors, and the nominal ratio of galaxy-to-total emission $L_{\rm gal}/L_{\rm tot}$. The sixteen quasars with detected hosts have redshifts ranging from $z = 0.6$ to $z = 2.3$, $L_{\rm gal}/L_{\rm tot}$ ratios from 20 to 80% and galaxy magnitudes $K_{\rm gal} = 15.2 - 17.8$, with the latter value roughly corresponding to the detection limit.

In Figure 4 we plotted the apparent K magnitudes versus redshift of the detected B3-VLA quasar hosts and the corresponding lower limits for those classified as point sources. For comparison we also plotted the K magnitudes of the RQ hosts detected by L92 and T96. L92 galaxy magnitudes were corrected to account for the galaxy flux missed in the inner-most 2 arcsec^2 area due to the PSF substraction. Following the author's estimations of a few tenths of magnitude correction, a correction of 0.4 magnitudes was applied. The brightest cluster galaxies (hereafter BCGs) in the redshift range $0.5 < z < 1.0$ studied by Aragón-Salamanca et al. (1993) are also shown. Although the classification of a galaxy as BCG is a relative one - the brightest of the cluster - these galaxies are similar in most properties to gEs.

The thin continuous curve in Fig. 4 shows the $K - z$ relation for 3CR and B2-1Jy class radio galaxies obtained by Lilly et al. (1985) and Lilly (1989), and the superimposed vertical line marks its dispersion, of 0.4 mag in the redshift range $1 < z < 2$. The dotted curve shows the $K - z$ relation expected for a passively-evolving old and luminous gE, in which all star formation has taken place during an initial burst, followed by no further star formation. This model reproduces very well the $K - z$ relation found by Lilly et al. (1985) and Lilly (1989) for RGs, and in fact this agreement has been traditionaly one of the main arguments for the interpretation of RGs as old passively evolving gEs. The modelled $K - z$ relation was obtained using Bruzual (1983) c-model and the recent implementation

of their code GISSEL (Galaxy Isochrone Synthesis Spectral Evolution Library, Bruzual & Charlot 1993, new version of 1995). The c-model assumes a constant star formation for an initial period τ and zero star formation thereafter. We used $\tau = 1$ Gyr, $M_{\rm K} = -25.8$ - which is the absolute magnitude of a BCG/gE for this cosmology (Thuan & Puschell 1989; Aragón-Salamanca et al. 1993) - and $z_{\rm for} = 10$, which for the adopted cosmology corresponds to an age of 12.6 Gyr for a present day galaxy. For this value of $z_{\rm for}$ the assumed star formation, lasting $\tau = 1$ Gyr, would have concluded at $z = 3.5$. The initial mass function used was a Salpeter IMF (1955), with M from 0.1 to 125 $M_{\odot}$.

In a recent work Eales & Rawlings (1996) reported a slightly fainter $K - z$ relation for their sample of B2-1Jy and 6C RGs. This relation is plotted as a dashed curve in Figure 4 and has a dispersion around 0.6 mag in the redshift range $1 < z < 2$. As noted by the authors, this relation is well matched with a c-model with similar parameters $\tau = 1$ Gyr and $M_{\rm K} = -25.8$, but assuming no stellar evolution. Since the stellar population must be evolving to some extent, the match with a non-evolving model is explained by the authors suggesting that the effect of stellar evolution is cancelled out by some process which makes the galaxy luminosity increase with age, as for instance the scenario of hierarchical clustering. The dash-dotted curve shows the no-evolution model. The thick curve shows the average $K - z$ relation for Lilly et al. and Eales & Rawlings. The former sample includes 3CR RGs with $S_{408} > 5$ Jy and B2-1 Jy sources with 1Jy $< S_{408} <$ 2 Jy. The RGs in the sample studied in Eales & Rawlings have flux densities in the range 0.8Jy $< S_{408} <$ 1.6 Jy. The flux densities of the B3-VLA quasars occupy an intermediate position between the two samples, with a median flux density around 2 Jy. Obviously, a better comparison of the host luminosities with those of RGs will be possible when K-band imaging of a complete sample of RGs selected from the B3 catalogue becomes available.

At low redshift ($z < 1.0$) there is a good agreement between the location of the detected

B3 quasar hosts and RGs/gEs, as well as with the BCGs studied by Aragón-Salamanca et al. (1993). There is one quasar at $z \simeq 0.5$, classified as point source, for which the upper limit for the host luminosity is much fainter than the typical luminosity of RGs and detected quasar hosts at these redshifts. A possible explanation for the inferred low luminosity is that the quasar is hosted by a compact galaxy, which could not be separated from the nucleus in our analysis. At high redshifts ($z > 1.0$) the detected B3-VLA quasar hosts tend to be brighter than RGs/gEs, and this trend is also found, although to a lesser extent by L92. We note, however, that our detection limit, $K \simeq 17.9$, prevents the identification of galaxy hosts near the expected location for RGs at $z \gtrsim 1.0$, and therefore only the galaxies brighter than this relation are expected to be detectable in our survey at these redshifts. In fact, eight of the sources with $z > 1.0$ in Fig. 4, comprising two weak galaxy detections and six lower limits, have galaxy magnitudes (or limits) consistent with the expected values for RGs. But the eight detected host galaxies with $z > 1.0$ (the two weak detections excluded) are clearly more luminous than typical RGs, deviating in seven cases more than 2σ relative to the $K - z$ relation by Lilly et al. (1985). The latter detections indicate that the B3 quasar hosts can reach higher luminosities than typical RGs/gEs, although the data imply a similar fraction of hosts having K magnitudes consistent with those of RGs/gEs.

A possible explanation for the largest luminosity of the detected hosts at $z > 1$ is that they are gEs, similar to RGs, except for a larger mass, i.e. intrinsic luminosity. This interpretation would imply that RQ hosts have a range of possible masses, since as shown in Fig. 4, the low redshift RQ hosts and some high redshift lower limits are consistent with having a mass similar to typical RGs/gEs. As we shall see below, under the assumption of passive stellar evolution, i.e. stellar evolution with no additional star formation after an initial burst, the largest luminosities obtained are not unreasonable, since they correspond to the bright end of the luminosity functions derived from galaxy surveys selected in the K band.

A second possibility is that these galaxies are gEs similar to RGs, but formed more recently. The long-dash-short-dash curves on Fig. 4 show the $K-z$ relation for c-models with $\tau = 1$ Gyr, $z_{\rm for} = 2, 3, 5$ and assumed stellar evolution. Especially the model with $z_{\rm for} = 3$ shows a good agreement with the data. For these models, the star formation, lasting 1 Gyr, ends at redshifts $z = 1.2, 2$ and 2.8, which roughly correspond to the minima in the $K-z$ curves. The large K band luminosity in these models is due to the contribution of massive red giants and supergiants. Since RQs do exist at larger redshifts, in these models different RQs would require different formation epochs. A problem with these models is that they appear to be inconsistent with the total B magnitudes measured for some of the quasars. For instance, using the model with $z_{\rm for} = 3$, the two well defined galaxies (filled circles) with $z > 2$, 0756+406 and 1142+392, would have blue colours, $B - K \simeq 2$ mag, implying $B_{\rm gal}$ about 19.1 and 18.7 respectively, and these values are lower in the first case and similar in the second case to the total quasar magnitudes in B (including the central QSO), of 19.9 and 18.8 magnitudes respectively.

A third possibility is that they are old gEs, similar in mass and age to RGs, but undergoing a large late starburst, probably related to the nuclear activity. The excess of K emission of the luminous galaxies relative to the $K-z$ relation for typical RGs is roughly $\Delta K \simeq 1.5$ mag and the derived starburst contribution would be $K_{\rm SB} \simeq 17$ mag. Assuming a flat spectrum during the starburst (Bruzual & Charlot 1993; Lilly 1989), corresponding to $B - K \simeq 2$ mag, the expected contribution in the B-band would be typically $B_{\rm SB} \simeq 19$ mag. Six of the eight RQs harboured by luminous galaxies have total B magnitudes (including the nuclear contribution) larger (four cases) or similar (two cases) than the expected value for $B_{\rm SB}$, rejecting this model as a possible general interpretation for the luminous galaxies.

We have calculated the absolute K magnitudes at $z = 0$ of the B3-VLA quasar host galaxies, assuming that through the whole redshift range the K emission is produced by a

mature population of passively-evolving stars. Although models involving young galaxies could be valid for some sources, they can be disregarded as a general interpretation, since they predict for the youngest sources a galaxy flux in B which is larger than the total flux measured for the quasar (nucleus included). The same occurs for the model in which *all* the K excess relative to a typical gE is attributed to young stars, since it also would predict B fluxes for the galaxies which would be generally larger than observed. An additional problem of these models is that they include unknown parameters such as the epoch and duration of the star formation period relative to the age of the galaxy, which would strongly affect the derived absolute magnitudes. In any case, for the galaxies with some degree of current star formation or formed at $z < 10$ the derived absolute magnitudes at $z = 0$ under the hypothesis of passive stellar evolution would be lower-limits. The absolute K magnitudes were calculated using the k and evolutionary corrections obtained from GISSEL for the c-model with $\tau = 1$ Gyr and $z_{\rm for} = 10$. k-corrections, evolutionary corrections and absolute K magnitudes of the sixteen galaxies are listed in Table 3. For the redshifts of the hosts, from $z = 0.6$ to $z = 2.3$, the $k + e$ corrections range from about –1.10 to about –2.5 mag.

In Figure 5a we plot the absolute magnitudes so obtained, $M_{\rm K}$ versus redshift for the detected RQ hosts in our work and those in T96 and L92. The curve corresponds to our maximum limiting magnitude for the detection of a host galaxy, $K = 17.9$. The absolute magnitudes of the B3 quasar hosts with $0.6 < z < 1.0$ are in the range $-26.0 \lesssim M_{\rm K} \lesssim -24.7$, showing a good agreement with the average absolute magnitudes of the RQ hosts in T96 sample between apertures $r = 12$ arcsec and $r = \infty$, and with those of the $0.5 < z < 1.0$ BCGs of Aragón-Salamanca et al. (1993), with $M_{\rm K} = -25.7 \pm 0.3$, as expected from Fig. 4. For comparison Thuan & Puschell (1989) found a slightly lower value $M_{\rm K} = -26.0$ for BCGs at $z < 0.1$. We note that the faint end of the absolute magnitude distribution for our data, $M_{\rm K} \simeq -24.7$, may be related to the detection limit in our analysis.

For this model, the detected RQ hosts in our sample with $z > 1$ have absolute magnitudes in the range $-27.5 < M_K < -26.5$. The corresponding absolute magnitudes for L92 RQ hosts would be slightly fainter, in the range $-27.0 < M_K < -26.0$ (excluding the galaxy with a large error), but their faintest sources would be undetectable or only marginally detectable in our work. The bright absolute magnitudes measured for the high redshift sources in our work $-27.5 < M_K < -26.5$ correspond to the bright end of the K-band luminosity function obtained for the E/S0s galaxies in the Anglo Australian Redshift Survey (Mobasher et al. 1986, redshifts in the range $0 < z < 0.11$), and for the recent K-band surveys by Glazebrook et al. (1996), up to $z \sim 0.8$ and Gardner et al. (1997) up to $z \sim 0.3$.

Considering the whole redshift range, the absolute K magnitudes of RQ hosts show some correlation with redshift, in the sense that lower redshift hosts ($z < 1$) do not reach as large luminosities at K as can be reached by high redshift hosts. This result has the implicit assumption that the K emission arises from a mature elliptical galaxy, which appears to be the most favoured model for the B and K band data. Although star formation cannot account for *all* the excess of K emission of the $z > 1$ galaxies, relative to typical gEs, it may produce part of this excess.

In Figure 5b we plot $M_{\rm K}$ versus redshift for the same sources, but using the no-evolution model (only k-correction), which matched the sample of RGs studied by Eales & Rawlings (1996). For the low redshift sources ($0.6 < z < 1.0$) the absolute magnitudes of the B3 quasar hosts are in the range $-26.5 \lesssim M_{\rm K} \lesssim -25.2$, showing a better agreement with the value $M_{\rm K} = -26.0$ found by Thuan & Puschell (1989) for BCGs at $z < 0.1$. However, the absolute magnitudes derived for the the high redshift sources for this model, in the range $-29.0 \lesssim M_{\rm K} \lesssim -27.5$, are by far more luminous than the brightest galaxies known from K-band surveys. For this reason we believe it is more appropriate to use the model with

stellar evolution, which yields absolute magnitudes for the RQ hosts similar to those of the brightest galaxies known.

So far we have tried to explain the high K-band luminosity of some of the RQ hosts galaxies using models of an ideal unperturbed galaxy for which we varied the mass or luminosity, the formation epoch or introduced renewed star formation. An alternative explanation to these high absolute magnitudes comes from the suggestion that the activity in radio sources is triggered by merging processes involving massive galaxies (see the reviews by Barnes & Hernquist, 1992, and others in Shlosman, 1994). There is in fact circumstancial evidence, up to $z \simeq 0.5$, that a large fraction of RQ hosts undergo tidal interactions/merging processes (Smith et al. 1986; Hutchings 1987; Disney et al. 1995; Hutchings & Neff 1997). In this case, the very process of galaxy interaction would naturally allow for a wide range of luminosities, depending on the luminosities of the interacting/merging galaxies. Some induced star formation could be also related to the interacting/merging process.

It is crucial to obtain high spatial resolution images of the detected B3-VLA quasar hosts to study their morphologies in more detail. Such images would allow to better determine the contribution of extended emission due to synchrotron and/or alignment effect, which is estimated to be low in the infrared for $z \sim 1$ RGs and RQ hosts. The study of the optical-infrared SED of the host galaxies is also necessary to better constraint the evolutionary models.

5. $B - K$ COLOURS OF THE QUASARS

In Paper I the study of the integrated $B - K$ colours of this sample of B3-VLA quasars was presented. The colours were obtained using the B magnitudes of the quasars taken from the catalogue of objects on the POSS-I blue plates generated by the APM

(accuracy 0.3 mag rms) and the K magnitudes measured from the images (both in Table 1). The distribution of $B-K$ colours for the B3 quasars (shown in Fig. 1a of Paper I) is similar in breadth to that found by Webster et al. (1995, hereafter W95) for flat-spectrum ($\alpha_{2700}^{5000} > -0.5$) radio-selected quasars (their Fig. 1b), except for the lack of extreme red colours $B-K > 6$. W95 interpreted the dispersion in the $B-K$ colour of their quasars ($1 < B-K < 8$) in terms of dust reddening, implying an extinction in the blue of several magnitudes for a substantial fraction of the quasars.

In Paper I we provide evidence that for most of the red B3-VLA quasars, the red colour is due to additional light in K (starlight or synchrotron emission) rather than a deficit in B due to dust extinction. The arguments for this interpretation are explained below and they are illustrated in figures 1a ($B-K$ histogram) and 2 ($K-z$ diagram) of Paper I. Many of the reddest B3 quasars have non-stellar images in K, consistent with the presence of underlying galaxies, and indeed many of the B3 quasars have K magnitudes which are not much brighter than their host galaxies are expected to be, assuming giant ellipticals with $M_K \sim -26$. Although the $B-K$ distribution for the flat and steep-spectrum quasars in our sample is not significantly different, of the six sources with the flattest spectra ($\alpha > -0.3$) only one has $B-K < 3.5$. These red colours are consistent with the presence of an enhanced synchrotron emission due to relativistic beaming, peculiar to flat-spectrum quasars, which extends to the optical and infrared (Bregman et al. 1981; Rieke et al. 1982; Browne & Murphy 1987). Serjeant & Rawlings (1996) have recently argued that such non-thermal emission may explain the red colours found by W95. The lack of quasars with $B-K > 6$ (W95 found several) in the B3-VLA Quasar Sample, dominated by steep-spectrum sources, is consistent with this interpretation. Additional support to the hypothesis that the reddening was due to a K excess came from the fact that two objects which stand out as being particularly luminous in K were also very red (see in Fig. 2 of Paper I the objects with $B-K = 5.6$ (flat) and $B-K = 4.4$, both with $K < 14$). These

sources are shown in Fig. 1b of the present work with underlined symbols.

Figure 6a shows the $B-K$ colour versus redshift for the 52 B3-VLA quasars. The distribution is similar to that found by W95, except for the lack of very red quasars ($B-K>6$). The average $B-K$ colour for the whole sample, consisting predominantly of steep-spectrum quasars, is $B-K=3.3\pm1.1$.

In total we have found eighteen B3-VLA quasars for which the K images show non-stellar profiles (see Sects. 3.2 and 3.3). For sixteen of them the light distribution is well fitted by models consisting of a QSO nucleus plus a host galaxy and the magnitudes of both components could be determined (rms around 0.4 mag). Twelve additional quasars were classified as point sources from the analysis in Sect. 3.2, and thus for these sources $K_{\rm QSO}=K$. Hence for these 28 sources we can study the intrinsic $B-K$ colours of the QSO, provided that the assumption can be made that most of the B emission arises from the QSO. The model of an old elliptical galaxy ($z_{\rm for}=10$), which is the model that better explains the properties of RQ hosts and RGs (Véron-Cetty & Woltjer 1990; Disney et al. 1995; T96; Ridgway & Stockton 1997; Lilly et al. 1985; Lilly 1989; Rigler et al. 1992; Best et al. 1997), has $B-K>6.0$ for the whole redshift range of our data, implying $B\sim22$ for the brighter galaxies, with $K\simeq16$, and even fainter B magnitudes for the rest. These B magnitudes are well below the typical total B magnitudes of the B3-VLA quasars (see Fig. 1), indicating that the relative galaxy contribution in B would be very small. Although the measured B and K fluxes rule out the model of an old galaxy with a large late starburst and the model of a young galaxy ($z_{\rm for}<5$), the data cannot reject, however, the presence of some low-level star formation, producing some contribution in B, similar to that found in FRII RGs (Heckman et al. 1986). In addition, some contribution in B could arise from scattered QSO light, a process which has also been observed in some RGs (e.g. di Serego Alighieri et al. 1989). In this section we study the intrinsic $B-K$ colours of the

twenty-eight quasars with determined $K_{\rm QSO}$, assuming that most of the quasar emission in B arises from the central QSO. The fact that the sources were identified in the POSS plates as pointlike lends additional support to this assumption. Hereafter $B-K$ will refer to the quasar colour and $B-K_{\rm QSO}$ to the QSO colour. Figures 6b and 6c show respectively the $B-K$ colour and $B-K_{\rm QSO}$ colour versus redshift for the twenty-eight sources with determined $K_{\rm QSO}$.

For the redshift range of this quasar sample, $0.4 < z < 2.3$ the K band corresponds to rest-frame regions from 1.6 μm to 6700 Å (or $14.30 < \log \nu < 14.65$) and B corresponds to 3000–1300 Å (or $15.00 < \log \nu < 15.35$). The average SED of QSOs is well fitted by a power law, with $S_\nu \propto \nu^\alpha$, with a break at rest-wavelength around 1 μm ($\log \nu = 14.5$), in which the spectral index steepens from high to low frequencies (Neugebauer et al. 1987; Sanders et al. 1989; Elvis et al. 1994). Although this general shape is well established, the dispersion around the average is rather large. The mean $\alpha_{\rm opt}$, at $\log \nu > 14.5$, is estimated to be around -0.2 (Neugebauer et al. 1987). For $\alpha_{\rm NIR}$, at $\log \nu < 14.5$, Neugebauer et al. quote -1.4. The typical SED of a radio quasar shown by Elvis et al. (1994, their Fig. 1) has a lower $\alpha_{\rm NIR}$, closer to -1, which is also the value used by Sanders et al. (1989).

Figure 7 shows the average rest-frame SED of QSOs using $\alpha_{\rm NIR} = -1$ and $\alpha_{\rm opt} = -0.2$. The rest-frame wavelengths at B and K for several redshifts are marked in the plot, using circles for K and squares for B. The redshifts are labelled.

For the quasars with $z > 1.3$, both B and K sample the optical range, i.e. $\log \nu > 14.5$. Assuming a constant spectral index, $\alpha_{\rm opt}$, we would expect a constant $B-K_{\rm QSO}$ colour, which does not change with redshift. The average $B-K_{\rm QSO}$ colour for the 11 QSOs in Fig. 6c with $z > 1.3$ is $B-K = 2.5 \pm 1.2$, which corresponds to $\alpha_{\rm opt} = -0.22$, in good agreement with Neugebauer et al. (1987) and Elvis et al. (1994). A dotted line indicates this average colour in Fig. 6c.

As we move to $z < 1.3$ in Fig. 7 the K band starts to sample infrared frequencies, below the frequency break at $\log \nu = 14.5$, and the slope corresponding to the $B - K_{\rm QSO}$ colour steepens, i.e. the $B - K_{\rm QSO}$ colour turns redder (see the dashed lines in Fig. 7). This result is consistent with our data, since the $B - K_{\rm QSO}$ colour for the QSOs with $z < 1.3$ is in average redder, with $B - K_{\rm QSO} = 3.2 \pm 1.2$. A dotted line in Fig. 6c shows this average. This $B - K_{\rm QSO}$ colour corresponds to an spectral index $\alpha = -0.64$, which is an upper limit to $\alpha_{\rm NIR}$, since the B band samples frequencies higher than the break. (It is obvious from Fig. 7 that $\alpha_{\rm NIR}$ is steeper than the slopes shown as dashed lines). Neugebauer et al. (1987) and Elvis et al. (1994) give $\alpha_{\rm NIR}$ in the range -1.4 to -1, consistent with our upper limit at $\alpha = -0.64$.

The effect of the removal of the host galaxy on the $B - K$ colours can be appreciated comparing these colours in Figures 6b and 6c. Considering the extended sources only, the average $B - K$ colour is reduced from 3.5 to 2.8 for $z < 1.3$ and from 2.9 to 1.9 for $z > 1.3$.

The 2σ dispersion of the $B - K_{\rm QSO}$ colours in Fig. 6c is of 2.4 both for the QSOs with $z < 1.3$ and $z > 1.3$. This dispersion in the $B - K_{\rm QSO}$ colours limits the amount of reddening to rest-frame dust extinctions $A_{\rm V} < 1.5$, $A_{\rm V} < 1$ and $A_{\rm V} < 0.8$, at $z = 0.5$, $z = 1.0$ and $z = 2.0$ respectively, where we used the reddening law of Kinney et al. (1994) for the optical/UV and Rieke & Lebofski (1985) for the infrared. These $A_{\rm V}$ values should be taken as conservative limits, since one would expect some of the spread in the $B - K_{\rm QSO}$ colours to be intrinsic. The inferred extinctions are in agreement with the values obtained for other quasar samples selected in radio, X-rays or in the optical (Schmidt 1968; Smith & Spinrad 1980; Netzer et al. 1995; Boyle & di Matteo 1995; Rowan-Robinson 1995, Baker 1997). Figure 6d shows the $B - K$ colours versus redshift for the quasars for which we could not determine $K_{\rm QSO}$. The colour distribution is rather flat and excluding the two quasars showing spatial structure (plotted as squares, one of them very red) the average

$B-K$ colour of these sources is $B-K=3.0\pm1.3$. For most of these sources the analysis of extension described in Sect. 3 was not performed, since either the sources were observed the second night or although observed the first night they had or could have problems of guiding/focusing. Therefore we expect that some of these sources also present some galaxy contamination at K.

6. ABSOLUTE K MAGNITUDES OF THE QUASARS AND CORRELATIONS WITH RADIO LUMINOSITY

We have calculated the K absolute magnitudes of the nuclear components for the twenty eight quasars for which $K_{\rm QSO}$ could be determined. In order to correct to rest-frame K absolute magnitudes we assumed a spectral index $\alpha=-1$ in the near infrared, although for $z>1.3$ the value could be slightly higher (more flat, see Sect. 5 and Fig. 7). The assumption of a spectral index $\alpha=-1$ implies a null k-correction. The K absolute magnitudes of the QSOs are listed in Table 4. The last column of the table indicates whether the quasar was pointlike or had resolved extended emission. In Figure 8 we show the diagram $M_{\rm K,QSO}$ versus redshift for these quasars. The data clearly show luminosity evolution with redshift in the K band. The average $M_{\rm K,QSO}$ for the sources at $z<1$ is $M_{\rm K,QSO}=-27.6\pm0.9$, but values as high as $M_{\rm K,QSO}=-30$ are reached at $1<z<2$. It is interesting to note the location on the diagram of the quasar 1144+402, with $z=1$ and $M_{\rm K,QSO}=-30.8$. This quasar is pointlike, has a flat radio spectrum with $\alpha=0.06$, a very bright nucleus at K, and a very red colour $B-K=5.6$. This is the flat-spectrum quasar appearing underlined in Fig. 1b. It is evident that the red colour of this source is due to a K excess rather than a defect at B, and the K excess is probably related to the flat radio spectrum. The flat-spectrum sources appear to have brighter nuclei at K in this diagram than the steep-spectrum ones.

In any radio selected flux-limited sample there is a strong "artificial" correlation between radio luminosity and redshift. Hence, it is possible that the brighter nuclear luminosities at K at redshifts $z > 1$ are related to the stronger radio power at these redshifts. Figure 9 shows the rest-frame luminosity at 1.4 GHz versus redshift for the B3-VLA quasars studied in this work. We used the observed total flux densities at 1.4 GHz and assumed a power law with the spectral index α_{408}^{1460} given in Table 1 to make the k-corrections, of the form $\log\,(1+z)^{-1-\alpha}$. Figure 9 clearly shows the artificial correlation between radio power and redshift mentioned above.

In Figure 10 we plotted the radio power $P_{1.4\ \mathrm{GHz}}$ versus $M_{\mathrm{K,QSO}}$ for the B3-VLA RQs with measured K_{QSO}. We found in fact a correlation between the two parameters, with a Spearman coefficient of -0.57 (significance level of 99.85%). This correlation improves considering only the steep-spectrum sources, as some of the flat-spectrum sources deviate towards higher nuclear luminosities at K. The Spearman coefficient of the correlation for steep-spectrum sources is -0.71 with a significance level of 99.97% and corresponding to $L_{\mathrm{radio}} \propto L_{\mathrm{K,QSO}}^{0.75\pm0.15}$. This correlation remains significant in the flux-flux plane (Fig. 11a), and the latter is not induced by distance effects, as low and high redshift RQs are equally distributed, each group showing the same correlation and spread as the whole sample (Fig. 11b). The flux-flux correlation for steep-spectrum sources has a Spearman coefficient of 0.72 with 99.96% significance. Therefore the data favour a direct link between the K flux from the nucleus and the synchrotron radio emission, which is more tight for the steep-spectrum quasars. The correlation $M_{\mathrm{K,QSO}} - z$ shown in Fig. 8 is weaker than the correlations $P_{1.4\ \mathrm{GHz}} - M_{\mathrm{K,QSO}}$ and $P_{1.4\ \mathrm{GHz}} - z$ and it is most likely induced by these two correlations.

Figure 12 shows a plot of $P_{1.4\ \mathrm{GHz}}$ versus $M_{\mathrm{K,gal}}$ for the sixteen B3-VLA quasars for which the galaxy component was measured, via light profile fitting. $M_{\mathrm{K,gal}}$ was calculated under the assumption that the whole K emission was produced by the old stars of a

passively evolving galaxy. A Spearman test for $L_{\rm radio} - L_{\rm K,gal}$ gives only a weak correlation ($r = -0.49$, 94% confidence level), corresponding to $L_{\rm radio} \propto L_{\rm K,gal}^{0.6\pm0.3}$, and the correlation dissapears in the flux-flux plane (Fig. 13, $r = 0.39$, 87% confidence level). We believe that the weak $P_{1.4\ \rm GHz}$-$M_{\rm K,gal}$ correlation is real; although the magnitude limit for the detection of the host galaxies could account in part for the lack of sources in the upper-left region of the $P_{1.4\ \rm GHz}$ versus $M_{\rm K,gal}$ diagram, the absence of bright galaxies at low radio powers clearly indicates a real $L_{\rm radio} - L_{\rm K,gal}$ trend, in the sense that the brighter galaxies host the more powerful radio quasars. As we did for the $M_{\rm QSO} - z$ relation, we interpret the trend $M_{\rm gal} - z$ in Fig. 5a as induced by the relations $M_{\rm gal} - P_{1.4\ \rm GHz}$ and $P_{1.4\ \rm GHz} - z$. The parameters $M_{\rm K,QSO}$ and $M_{\rm K,gal}$ appear to be marginally correlated ($r = -0.45$, 92% confidence level) although the correlation dissapears in the $K_{\rm QSO} - K_{\rm gal}$ plane (Figures 14 and 15).

The trend $P_{1.4\ \rm GHz}$-$M_{\rm K,gal}$ indicates that powerful radio quasars inhabit the most massive galaxies. In particular, all the bright RQ hosts, with $M_{\rm K,gal} < -26$, have radio powers $P_{1.4\ \rm GHz} > 10^{27.5}$ WHz^{-1}. A similar tendency was found by Yates, Miller & Peacock (1986) for RGs. These authors selected a sample of FR-II 3C RGs and concluded that for the more powerful sources ($P_{178\rm MHz} > 10^{27}$ W Hz^{-1}) there is a correlation between the K absolute magnitude of the host galaxy and radio power. They suggested that the correlation is caused by the increase of stellar luminosities by cannibalism in the most powerful radio galaxies. As suggested by Baum, Heckman & van Breugel (1992) and Baum, Zirbel & O'Dea (1995) mergers at earlier epochs would have provided high angular momentum gas to fuel accretion onto the nucleus, producing an FR-II radio source or a quasar. If we translate our data to Figure 1 in Yates et al. (1986) we observe that the quasar hosts lie in the same region that the most powerful RGs and in fact both would be indistinguishable. This gives support to unification schemes of radio sources, where FR-II RGs are the parent population of radio quasars and both are expected to have similar relationships between

radio power and host galaxy properties.

7. SUMMARY AND CONCLUSIONS

We have obtained K-band images of a representatitve sample of 52 quasars with $0.3 < z < 2.8$, $S_{408\ \mathrm{MHz}} > 0.5$ Jy and radio powers $P_{1.4\ \mathrm{GHz}} \simeq 10^{27} - 10^{28}$ WHz^{-1}, whose analysis yield the following conclusions.

For sixteen out of 28 sources for which the images allowed a detailed morphological analysis, resolved extended emission was detected around the central QSO, with estimated apparent magnitudes in the range $K \simeq 15.5 - 17.5$. The redshifts of these QSOs with extended emission are in the range from 0.6 to 2.3. Interpreting this "fuzz" as starlight emission from the host galaxy, its location in the $K - z$ diagram for the low-redshift quasars, with $z \lesssim 1$, is consistent with these quasars being hosted by galaxies similar to gEs/RGs at these redshifts. At high redshifts, $z \gtrsim 1$, the extended emission reaches higher luminosities than those found for typical gEs/RGs at these redshifts, a trend which was also found although to a lesser extent by L92. Since at $z \gtrsim 1$ a typical gE has apparent magnitudes in K near the detection limit for our analysis, only the most luminous galaxies are detectable in our work at these redshifts.

We have considered three possible explanations for the large luminosities of the detected host galaxies with $z \gtrsim 1$: mature elliptical galaxies with masses larger than a typical gE; young elliptical galaxies, formed at $z \simeq 2 - 4$, with present-day K luminosity similar to gEs; and mature galaxies similar in mass to gEs but undergoing a recent starburst. The two last models cannot be taken as a general interpretation of the luminous galaxies, since they predict for many of the sources a larger B flux from the galaxy than the total B flux measured for the quasar, including host and nucleus. The most appropriate model to

account for both the K and B band data for the majority of the sources is that of a mature passively evolving elliptical galaxy with a range of possible masses. Using this model we derive a present-day absolute K magnitude, $M_{\rm K} \simeq -26$, for the B3-VLA quasar hosts at $z \lesssim 1$, similar to the typical values found for RGs. The absolute magnitudes we obtain for the high redshift B3-VLA quasar hosts, $M_{\rm K} \simeq -27$, correspond to the bright end of the K-band galaxy luminosity functions obtained from galaxy surveys selected in this band (Mobasher et al. 1996; Glazebrook et al. 1996; Gardner et al. 1997). Rephrasing L92, " the host galaxies of RQs at any redshift are probably a subset of the most massive galaxies in existence". A possible explanation of these large luminosities is that the host galaxies of RQs are the product of a past merger event. This process would also contribute to the triggering of the nuclear activity.

From a quantitative analysis of the $B - K_{\rm QSO}$ colour of the B3-VLA quasars for which the nuclear component could be measured, we confirmed our previous conclusion, based on the integrated quasar $B - K$ colours (Paper I), that the $B - K$ colours of the nuclear component show a small dispersion, of about 2.4 mag. This small dispersion in the $B - K$ colour imply a low reddening, $A_{\rm V} < 1.0$ at $z \simeq 1$ similar to that found for other quasar samples selected in the optical, radio, or X-rays.

We have found a correlation between radio power and nuclear K-band luminosity, indicating a direct link between the nuclear infrared emission and the radio synchrotron emission. The correlation is more tight for the steep-spectrum sources (99.97% significance). In addition a relation between radio power and infrared luminosity of the host galaxy is found, in the sense that the most luminous (massive) host galaxies contain the most powerful RQs. It would be interesting to increase the number of B3-VLA quasars with measured hosts, through obtaining new $K-$band images, to confirm this trend. A similar result was found for powerful FR-II RGs by Yates et al. (1986), who suggested that the

trend is caused by the increase of stellar luminosities by cannibalism in the most powerful RGs. The similarity of the relations between radio power and galaxy luminosity found for FR-II RGs and RQs supports the unification between the two populations.

Acknowledgements.

We have made use of the APM Catalogues. We thank the referee, R. Antonucci, for valuable comments and suggestions which improved the paper. We also thank S. Charlot for providing us with the GISSEL package, and L. Cayón and I. Ferreras for their help in obtaining the k and evolutionary corrections from the GISSEL models. The William Herschel Telescope is operated by the Royal Greenwich Observatory at the Spanish Observatorio del Roque de Los Muchachos of the Instituto de Astrofísica de Canarias on behalf of the Science and Engineering Research Council of the United Kingdom and the Netherlands Organization for Scientific Research. Financial support was provided under DGICYT project PB92-0501, DGES project PB95-0122 and by the Comisión Mixta Caja Cantabria-Universidad de Cantabria.

REFERENCES

Antonucci, R. 1993, ARA&A, 31, 473

Aragón-Salamanca, A., Ellis, R.S., Couch, W.J., & Carter, D. 1993, MNRAS262, 764

Bailey, M.E., & Sparks, W.B. 1982, MNRAS, 204, 53p

Baker, A.C., Carswell, R.F., Bailey, J.A., Espey, B.R., Smith, M.G., Ward, M.J., 1994, MNRAS, 270, 575

Baker, J.C., Hunstead, R.W., 1995, ApJ, 452, L95

Baker, J.C., 1997, MNRAS, 286, 23

Barnes, J.E., & Hernquist, L. 1992, ARA&A, 30, 705

Baum, S.A., Heckman, T.M., & van Breugel, W. 1992, ApJ, 389, 208

Baum, S.A., Zirbel, E.L., & O'Dea, C.P. 1995, ApJ, 451, 88

Benn, C.R., Vigotti, M., Carballo, R., González-Serrano, J.I., & Sánchez, S.F. 1997, MNRAS, in press (Paper I)

Best, P., Longair, M., & Röttgering, H. 1997, in *Galaxy Scaling Relations: Origins, Evolution and Applications*, ed. L. da Costa. In press (SISSA preprint, astro-ph/9703055)

Boroson, T.A. & Oke, J.B. 1984, ApJ, 281, 535

Boroson, T.A., Persson, S.E., & Oke, J.B., 1985, ApJ, 293, 120

Boyle, B.J., & di Matteo, T. 1995, MNRAS, 277, L63

Bregman, J.N., *et al.*, 1981, Nature, 293, 714

Browne, I.W.A., & Murphy, D.W. 1987, MNRAS, 226, 601

Bruzual, G. 1983, ApJ, 273, 105

Bruzual, G., & Charlot, S. 1993, ApJ, 405, 558

Capaccioli, M., & de Vaucouleurs, G. 1983, ApJS, 52, 465

Chambers, K.C., Miley, G.C., & van Breugel, W.J.M. 1987, Nature, 329, 624

Cimatti, A., Dey, A., van Breugel, W., Hurt, T., & Antonucci, R. 1997, ApJ, 476, 677

Dey, A., van Breugel, W., Vacca, W.D., & Antonucci, R. 1997, ApJ, in press (SISSA preprint, astro-ph/9707166)

di Serego Alighieri, S., Fosbury, R.A.E., Quinn, P.J., & Tadhunter, C.N., 1989, Nature, 341, 307

Disney, M.J., *et al.* 1995, Nature, 376, 150

Dunlop, J.S., Taylor, G.L., Hughes, D.H., & Robson, E.I. 1993, MNRAS, 264, 455

Eales, S.A., & Rawlings, S. 1996, ApJ, 460, 68

Elvis, M., *et al.* 1994, ApJS, 95, 1

Glazebrook, K., Peacock, J.A., Miller, L., & Collins, C.A. 1995, MNRAS, 275, 169

González-Serrano, J.I., Carballo, R., & Pérez-Fournon, I. 1993, AJ, 105, 1710

Heckman, T.M., *et al.* 1986, ApJ, 311, 526

Heckman, T.M., Lehnert, M.D., van Breugel, W., & Miley, G.K. 1991, ApJ, 370, 78

Hutchings, J.B. 1987, ApJ, 320, 122

Hutchings, J.B., & Neff, S.G. 1997, AJ, 113, 550

Irwin, M. 1992, Gemini 37, 1. Newsletter of the Royal Greenwich Observatory

Jedrzejewski, R.I. 1987, MNRAS, 226, 747

Kapahi, V.K., McCarthy, P.J., Athreya, R.M., van Breugel, W. & Subrahmanya, C.R. 1996, in *Extragalactic Radio Sources*, 517, eds. R. Ekers, C. Fanti & L. Padrielli. Kluwer Academic Publishers.

Kinney, A.L., Calzetti, D., Bica, E., & Storchi-Bergmann, T. 1994, ApJ, 429, 172

Laing, R.A., Riley, J.M., & Longair, M.S. 1983, MNRAS, 204, 151

Large, M.I., Mills, B.Y., Little, A.G., Crawford, D.E., & Sutton, J.M. 1981, MNRAS, 194, 693

Lehnert, M.D., Heckman, T.M., Chambers, K.C., & Miley, G.K. 1992, ApJ, 393, 68 (L92)

Lilly, S.J., & Longair, M.S. 1982, MNRAS, 199, 1053

Lilly, S.J., & Longair, M.S. 1984, MNRAS, 211, 833

Lilly, S.J., Longair, M.S., & Allington-Smith, J.R. 1985, MNRAS, 215, 37

Lilly, S.J. 1989, ApJ, 340, 77

Lilly, S.J. 1993, in *The Environment and Evolution of Galaxies*, 143, eds. J.M. Shull & H.A. Thronson. Kluwer Academic Publishers.

Lucy, L.B. 1974, AJ, 79, 745

Lucy, L.B. 1992, AJ, 104, 1260

McCarthy, P.J. 1993, ARA&A, 31, 639

McCarthy, P.J., van Breugel, W.J.M., Spinrad, H., & Djorgovski, S. 1987, ApJ, 321, 29

McCarthy, P.J., Kapahi, V.K., van Breugel, W., Persson, S.E., Athreya, R.M., & Subrahmanya, C.R. 1996, ApJS, 107, 19

McLeod, K.K., & Rieke, G.H. 1995, ApJ, 454, 77

Mobasher, B., Ellis, R.S., & Sharpless, R.M. 1986, MNRAS, 223, 11

Netzer, H., Brotherson, M.S., Wills, B.J., Han, M., Wills, D., Baldwin, J.A., Ferland, G.J., & Browne, I.W.A. 1995, ApJ, 448, 27

Neugebauer, G., Green, R.F., Matthews, K., Schmidt, M., Soifer, B.T., & Bennett, J. 1987, ApJS, 63, 615

Osterbrock D.E., 1989, in *Astrophysics of Gaseous Nebulae and Active Galactic Nuclei*. University Science Books

Richardson, W.H. 1972, J. Op. Soc. Am. 62, 52

Ridgway, S.E., & Stockton, A. 1997, AJ, 114, 511

Rieke, G.H., Lebofsky, M.J., & Wisniewski, W.Z. 1982, ApJ, 263, 73

Rieke, G.H., & Lebofsky, M.J. 1985, ApJ, 288, 618

Rigler, M.A., Lilly, S.J., Stockton, A., Hammer, F., & Le Fevre, P. 1992, ApJ, 385, 61

Rigler, M.A., & Lilly, S.J. 1994, ApJ, 427, 79

Rönnback, J., van Groningen, E., Wanders, I., & Örndahl, E. 1996, MNRAS, 283, 282

Rowan-Robinson, M. 1995, MNRAS, 272, 737

Salpeter, E.E. 1955, ApJ, 121, 161

Sanders, D.B., Phinney, E.S., Neugebauer, G., Soifer, B.T., & Matthews, K. 1989, ApJ, 347, 29

Shlosman, I., ed. 1994 *Mass-Transfer Induced Activity in Galaxies*. New York: Cambridge Univ. Press.

Schmidt, M. 1968, ApJ, 151, 393

Serjeant, S., & Rawlings, S. 1995, Nature, 379, 304

Smith, H.E., & Spinrad, H. 1980, ApJ, 236, 419

Smith, E.P., Heckman, T.M., Bothun, G.D., Romanishin, W., & Balick, B. 1986, ApJ, 306, 64

Spinrad, H., Djorgovski, S., Marr, J., & Aguilar, L. 1985, PASP, 97, 932

Stockton, A & Mackenty, J.W. 1987, ApJ, 316, 584

Taylor, G.L., Dunlop, J.S., Hughes, D.H., & Robson, E.I. 1996, MNRAS, 283, 930

Thuan, T.X., & Puschell, J.J. 1989, ApJ, 346, 34

Véron-Cetty, M.P., & Woltjer, L. 1990, A&A, 236, 69

Vigotti, M., Grueff, G., Perley, R., Clark, B.G., & Bridle, A.H. 1989 AJ, 98, 419

Vigotti, M., Vettolani, G.V., Merighi, R., Lahulla, J.F., & Pedani, M. 1997, A&AS, 123, 1

Webster, R.L., Francis, P.J., Peterson, B.A., Drinkwater, M.J., & Masci F.J. 1995, Nature, 375, 469

Yates, M.G., Miller, L., & Peacock, J.A. 1986 MNRAS, 221, 311

This manuscript was prepared with the AAS LaTeX macros v4.0.

Fig. 1.— Distribution of B and K magnitudes versus redshift for the 52 B3-VLA quasars studied in this work. Crosses correspond to flat-spectrum sources ($\alpha_{408}^{1460} > -0.5$, $S_\nu \propto \nu^\alpha$).

Fig. 2.— Surface brightness profile of B3 1111+408 obtained from the deconvolved image. The solid line is the best fit with a two-component model consisting of a nucleus (dash-dotted line) and an elliptical galaxy (dashed line).

Fig. 3.— Contour maps and surface brightness profiles of the extended sources. For each quasar panel (a) is a contour map of the original image; panel (a.1) is its corresponding brightness profile (dots) plotted with the PSF (solid line); (b) is a contour map of the nucleus-subtracted image and (b.1) its corresponding brightness profile. Orientation in the contour plots is north to the top and east to the left and the distance between tick marks is 2.7 arcsecs. Intensities are given in counts and the spacial axes are in pixels.

Fig. 4.— $K-z$ diagram for the B3-VLA quasar hosts, and other galaxies or RQ host galaxies from the literature. Circles show the detected B3-VLA hosts (empty circles corresponding to detections with weaker significance) and filled triangles lower limits to the host magnitudes. L92 RQ hosts are indicated as pentagons and squares represent T96 best fitted RQ hosts. Empty squares correspond to 12 arcsec aperture magnitudes and filled squares to total magnitudes estimated by the authors integrating the best-fit models to $r = \infty$. The BCGs in Aragón-Salamanca et al. (1993) are shown as stars. The thin continuous curve is the $K-z$ relation of Lilly et al., the short dashed curve is the same relation for B2-1Jy/6C RGs of Eales & Rawlings, and the thick curve is the average of both relations. The remaining curves correspond to models. The dotted curve is Bruzual & Charlot (1993) c-model for $z_{\rm for} = 10, \tau = 1$ Gyr and $M_{\rm K} = -25.8$, the dashed-dotted curve is a similar model but considering no stellar evolution, and the long-dash-short-dash curve shows models similar to the first one but using $z_{\rm for} = 2, 3, 5$.

Fig. 5.— Present day absolute K magnitude, $M_{\rm K,gal}$, versus redshift for the detected and measured B3-VLA quasar host galaxies and other galaxies or RQ host galaxies from the literature, assuming passive stellar evolution (a) or no-evolution (b). Symbols are the same as for Fig. 4. The curve corresponds to our maximum limiting magnitude for the detection of a host galaxy, $K = 17.9$.

Fig. 6.— $B - K$ colours versus redshift for the B3-VLA quasars. Flat-spectrum sources are indicated with crosses. Triangles show the pointlike sources and empty squares the two quasars showing spatial structure on the images. The quasars with a fitted galaxy component are shown in panels (b) and (c) as filled circles (significant detection) or empty circles (weak detection). The dotted lines in panel (c) show the average $B - K_{\rm QSO}$ colours for redshifts $z < 1.3$ and $z > 1.3$.

Fig. 7.— Standard mean SED of a QSO using $S_\nu \propto \nu^\alpha$ with $\alpha_{\rm opt} = -0.2$, $\alpha_{\rm NIR} = -1$ and the break at $\log \nu = 14.5$ (Neugebauer et al. 1987, Sanders et al. 1989, Elvis et al. 1994). Filled circles show the rest-frame frequencies observed in the K band at redshifts $z = 0$, $z = 0.5$, $z = 1.5$ and $z = 2.0$. Empty squares show the same data for the B band.

Fig. 8.— $M_{\rm K,QSO}$ versus redshift for the 28 quasars with determined $K_{\rm QSO}$. Symbols are similar as for figs. 4-6.

Fig. 9.— Radio power, $P_{1.4\ \rm GHz}$, versus redshift for the 52 B3-VLA quasars in this work. The curve shows the radio power $P_{1.4\ \rm GHz}$ corresponding to a flux limit $S_{408} = 0.6$ Jy and the average spectral index of the sample $\alpha_{408}^{1460} = -0.79$.

Fig. 10.— $P_{1.4\ \rm GHz}$ versus $M_{\rm K,QSO}$ for the 28 quasars with determined $K_{\rm QSO}$.

Fig. 11.— Total measured radio flux at 1.4 GHz versus $K_{\rm QSO}$ for the 28 quasars with determined $K_{\rm QSO}$. For panel (a) the symbols are similar to those used for figs. 4-6. For

panel (b) two different symbols are used to separate the sources in two redshift bins.

Fig. 12.— $P_{1.4\ \mathrm{GHz}}$ versus $M_{\mathrm{K,gal}}$ for the sixteen quasars with determined K_{gal}.

Fig. 13.— Total measured radio flux at 1.4 GHz versus K_{gal} for the 16 quasars with determined K_{gal}. For panel (a) the symbols are similar to those used for figs. 4-6. For panel (b) two different symbols are used to separate two redshift bins.